Composite scalar dark matter

Michele Frigerio,[a,b] **Alex Pomarol,**[c] **Francesco Riva**[d] **and Alfredo Urbano**[e]

[a] *CNRS, Laboratoire Charles Coulomb,*
UMR 5221, F-34095 Montpellier, France

[b] *Université Montpellier 2, Laboratoire Charles Coulomb,*
UMR 5221, F-34095 Montpellier, France

[c] *Departament de Fisica, Universitat Autònoma de Barcelona,*
08193 Bellaterra, Barcelona, Spain

[d] *IFAE, Universitat Autònoma de Barcelona,*
08193 Bellaterra, Barcelona, Spain

[e] *Laboratoire de Physique Théorique de l'École Normale Supérieure,*
24 rue Lhomond, F-75231 Paris, France

E-mail: michele.frigerio@um2.fr, pomarol@ifae.es, friva@ifae.es, urbano@lpt.ens.fr

Abstract: We show that the dark matter (DM) could be a light composite scalar η, emerging from a TeV-scale strongly-coupled sector as a pseudo Nambu-Goldstone boson (pNGB). Such state arises naturally in scenarios where the Higgs is also a composite pNGB, as in $O(6)/O(5)$ models, which are particularly predictive, since the low-energy interactions of η are determined by symmetry considerations. We identify the region of parameters where η has the required DM relic density, satisfying at the same time the constraints from Higgs searches at the LHC, as well as DM direct searches. Compositeness, in addition to justify the lightness of the scalars, can enhance the DM scattering rates and lead to an excellent discovery prospect for the near future. For a Higgs mass $m_h \simeq 125\,\text{GeV}$ and a pNGB characteristic scale $f \lesssim 1\,\text{TeV}$, we find that the DM mass is either $m_\eta \simeq 50-70\,\text{GeV}$, with DM annihilations driven by the Higgs resonance, or in the range $100-500\,\text{GeV}$, where the DM derivative interaction with the Higgs becomes dominant. In the former case the invisible Higgs decay to two DM particles could weaken the LHC Higgs signal.

Keywords: Higgs Physics, Cosmology of Theories beyond the SM, Technicolor and Composite Models

Contents

1 Motivation

From a theoretical point of view light scalar particles are unnatural, unless a suitable structure protects their mass from large quantum corrections. In the Standard Model (SM) there is a compelling case for a light scalar, the Higgs boson, and many efforts have been made to address the associated hierarchy problem. The dark matter (DM) energy density of the Universe could also be accounted for by a new light scalar. The minimal realization, extensively studied in the literature (see e.g. ref. [1–8]), consists in adding to the SM a gauge singlet real scalar η, and assuming that it is stable due to a parity $\eta \to -\eta$. The model is quite predictive since it only depends on two extra parameters: the singlet mass m_η and its "portal" coupling to the Higgs boson, λ. This apparent simplicity, however, calls for an ultraviolet completion. As we said, light scalars are unnatural in quantum field theories, unless they are accompanied by new ingredients, such as for example supersymmetry, and these deeply affect the dynamics of the DM.

Light scalars can also be natural if they are not elementary particles, rather composite states emerging from a strongly-coupled fundamental theory. Similarly as pions in QCD, light scalars can appear as pseudo Nambu-Goldstone bosons (pNGBs) arising from the spontaneous breaking of the global symmetries of the strong sector around the TeV scale.

A well-known example is the symmetry breaking pattern SO(5)/SO(4), that generates four pNGBs with the quantum numbers of the SM Higgs doublet H, the weak gauge group being embedded in SO(4) $\simeq$ SU(2)$_L$ × SU(2)$_R$ [9]. The most minimal extension to this symmetry pattern is the SO(6)/SO(5) model, that contains five pNGBs in the spectrum: the Higgs doublet H and a gauge singlet η [10]. Interestingly, the pattern SO(6)/SO(5) is the minimal example with a known ultraviolet completion in terms of techni-quarks [11].

The purpose of this article is to study under which conditions η is a suitable DM candidate. The properties of η, being a pNGB, are determined by the global symmetries of the strong sector, and by the way these symmetries are explicitly broken by the couplings of the SM fields to the strong sector. We will analyze the phenomenology of this composite DM particle and its interplay with the composite Higgs doublet H.

The DM couplings are substantially different from the non-composite singlet case. This is mainly due to new non-renormalizable interactions between η and the SM fields, arising from operators of dimension-six suppressed by $1/f^2$ where $f \sim \text{TeV}$ is the decay constant of the NGBs. There are two types of these interactions: (i) derivative couplings between η and H, fully determined by the SO(6)/SO(5) structure, that scale as p^2/f^2 where p is the relevant momentum in a given process, and (ii) direct couplings between η and the SM fermions, arising from the explicit breaking of the global SO(6) symmetry, that scale as $m_\psi p/f^2$ where m_ψ is the mass of the fermion. These interactions make the phenomenology of the composite scalar DM substantially different from that of an elementary scalar (similar candidates of composite scalar DM have been also proposed, for instance, in the context of techni-colour theories [12] and gauge-Higgs unified models [13]; see also ref. [14]).

In section 2 we present the effective lagrangian for the composite η, defined from symmetry considerations and naive dimensional analysis (NDA). In section 3 we compute the composite DM relic density. In sections 4 and 5 we study respectively the constraints coming from the Higgs searches at the LHC and the DM direct detection experiments. We combine these results in section 6, where we identify the regions of parameters that fulfill all the phenomenological requirements. We conclude in section 7 and leave the technical details of the composite models for appendix A, and the lengthy expressions for the relic density and direct detection cross sections for appendices B and C, respectively.

2 Light scalar dark matter from a composite sector

We consider theories with a light scalar sector consisting only of a Higgs doublet H and a singlet η with parity

$$\eta \to -\eta \,, \tag{2.1}$$

that makes η stable. The lightness of these states is a consequence of a global symmetry. The simplest realization consists of having a new strong sector with a global symmetry breaking pattern given by $O(6) \to O(5)$. Five NGBs emerge from this spontaneous breaking: a $\mathbf{5}$ of SO(5) which decomposes as $\mathbf{4} \oplus \mathbf{1} \simeq (\mathbf{2}, \mathbf{2}) \oplus (\mathbf{1}, \mathbf{1})$ under the subgroup SO(4) $\simeq$ SU(2)$_L$ × SU(2)$_R$. The $\mathbf{4}$ is identified with H, while the gauge singlet is η (see appendix A for details). Thinking of SO(6) as the rotation group in a six-dimensional space, the symmetry under which η shifts corresponds to a rotation in the 5-6 plane,

$SO(2)_{5-6} \equiv SO(2)_\eta \simeq U(1)_\eta$, while eq. (2.1) corresponds to the six-dimensional parity of $O(6)$, $P_\eta = \text{diag}(1,1,1,1,-1,1)$.

If it were for the strong sector alone, the pNGBs H and η would be massless and would only interact derivatively. However, the SM gauge bosons and fermions couple to the strong sector breaking explicitly $O(6)$, generating non-derivative interactions between H, η and the SM fields. We will assume that P_η is preserved by the SM couplings to the strong sector. At the one-loop level these couplings induce a potential for H and η, that is eventually responsible for electroweak symmetry breaking (EWSB), with $v \equiv \sqrt{2}\langle H \rangle = 246\,\text{GeV}$ and $\langle \eta \rangle = 0$.

This scenario, apart from giving a solution to the hierarchy problem, since the Higgs is naturally a light state, also provides a good candidate for DM, the extra state η, that is also naturally light. At energies below the strong scale, denoted by $m_\rho \sim$ few TeV, the lagrangian for η at the lowest order in a η^2/f^2 expansion, where f is the pNGB decay constant, is given by

$$\mathcal{L}_\eta = \frac{1}{2}(\partial_\mu \eta)^2 - V(\eta, H) + \frac{1}{2f^2}\left(\partial_\mu |H|^2 + \frac{1}{2}\partial_\mu \eta^2\right)^2 \tag{2.2}$$

$$+ \frac{\eta^2}{f^2}\left(c_t y_t\, \overline{q_L}\tilde{H}t_R + c_b y_b\, \overline{q_L}H b_R + h.c.\right) + \cdots, \tag{2.3}$$

where

$$V(\eta, H) = \frac{1}{2}\mu_\eta^2 \eta^2 + \lambda |H|^2 \eta^2 + \cdots. \tag{2.4}$$

For simplicity, only the interactions with the third family of SM quarks are shown, that are the ones that play the most prominent role. Let us remark that these operators are not suppressed by the mass of the heavy composite states m_ρ but rather by the smaller scale $f \sim m_\rho/g_\rho$ where g_ρ is the inter-composite coupling, expected to satisfy $1 \lesssim g_\rho \lesssim 4\pi$.

A few comments on the lagrangian in eqs. (2.2)–(2.4) are in order. The only interaction that preserves the Nambu-Goldstone shift symmetries is the derivative term in eq. (2.2) that, as shown in appendix A, is fully determined by the $SO(6)/SO(5)$ symmetry. The coefficients $c_{t,b}$, instead, depend crucially on how the fermions couple to the strong sector and break explicitly the $SO(6)$ symmetry. In general, we expect c_t (c_b) to be an $O(1)$ complex number whenever the $U(1)_\eta$ symmetry is broken by the q_L and/or by the t_R (b_R) coupling to the strong sector; otherwise they are zero. Both possibilities are realized in simple models, as described in appendix A. Notice that the interactions of eq. (2.3) can also be induced from operators of the form

$$\overline{q_L}\gamma^\mu \partial_\mu q_L \frac{\eta^2}{f^2}, \tag{2.5}$$

and similarly for t_R and b_R. Indeed, using the equations of motion for the fermion we can rewrite the above operator as those in eq. (2.3).

Let us briefly discuss the potential $V(\eta, H)$. It can only arise from loop effects involving the SM fields. Since the SM gauge interactions preserve the $U(1)_\eta$ symmetry, μ_η and λ can only be generated from fermion interactions that break $U(1)_\eta$. Since λ is further protected

by the symmetry under which H shifts, we generically expect

$$\lambda \lesssim \mu_\eta^2/f^2\,. \tag{2.6}$$

Then, the mass of η is given by $m_\eta^2 = \mu_\eta^2 + \lambda v^2 \simeq \mu_\eta^2$, since electroweak precision measurements require [15]

$$\xi \equiv \frac{v^2}{f^2} \ll 1\,. \tag{2.7}$$

It is easy to construct models where the $\mathrm{U}(1)_\eta$ symmetry is either broken by the top or the bottom coupling to the strong sector, giving a one-loop mass for η of the order of 500 or 50 GeV respectively, as shown in appendix A. We also notice that in the potential we have ignored terms beyond the quadratic order in the η field, since they do not play any important role in our DM analysis.

Apart from eq. (2.2) and eq. (2.3), there is also the possibility to have at order η^2/f^2 the interaction terms

$$\frac{\eta^2}{f^2} \sum_{F=B,W,G} \left(c_{F\eta} F_{\mu\nu} F^{\mu\nu} + \tilde{c}_{F\eta} F_{\mu\nu} \tilde{F}^{\mu\nu} \right)\,. \tag{2.8}$$

These couplings do not respect the $\mathrm{U}(1)_\eta$ symmetry and therefore can only be induced by loops involving heavy composite states that see the $\mathrm{U}(1)_\eta$-breaking through mixing with the SM states. We estimate them to be $c_{F\eta}, \tilde{c}_{F\eta} \sim (g_F/g_\rho)^2 (m_\eta/m_\rho)^2$, smaller than contributions coming from SM loops. We will neglect them from now on.

In summary, the interactions between our DM candidate η and the SM particles are controlled by four parameters: c_b, c_t, f and λ. For our DM analysis below we shall consider the following values for these parameters. Since the bottom quark plays a main role in the computation of the DM relic density, in order to highlight the effects of compositeness we will assume that its couplings to the strong sector break $\mathrm{U}(1)_\eta$, so that $c_b \neq 0$. More specifically, motivated by the models described in appendix A, we will consider the range

$$c_b = \frac{1}{2} + a + ib\,, \quad a,b \in [0,1]\,, \tag{2.9}$$

where small (large) values of a and b correspond to small (large) couplings of $b_{L,R}$ to the strong sector. For the top coupling c_t we will consider two cases:

- Case 1: $\mathrm{U}(1)_\eta$ is broken by the top and we fix for definiteness $c_t = 1/2$ as in minimal models (see appendix A). The top loops make η generically heavier than the Higgs.

- Case 2: The top interactions do not break $\mathrm{U}(1)_\eta$. We then have $c_t = 0$ and m_η does not receive contributions from top loops. In this scenario the DM particle η can be naturally lighter than the Higgs.

For the decay constant f we will take $f = 500$ GeV and $f = 1$ TeV. Recall that although composite Higgs models generically predict $f \sim v \simeq 246$ GeV, electroweak precision measurements require eq. (2.7) to hold. Finally, we will leave λ and m_η as free parameters to be determined by the requirement of η to be a realistic DM candidate.

The couplings of η to the 1st and 2nd family quarks will be important only when considering direct DM detection. If not otherwise specified, we will assume for simplicity family independent coefficients, $c_u = c_c = c_t$ and $c_d = c_s = c_b$. This choice is partly motivated by the bounds on flavour violation [10].

To recover the predictions of the renormalizable model [1–8], that we will refer to as the 'non-composite case', we can take the limit $f \to \infty$. In this case only λ controls the interactions of η with the SM fields.

3 Relic density of the composite dark matter

In the standard cosmological framework, DM was kept in thermal and chemical equilibrium as a consequence of its interactions with the SM particles. As the Universe expanded and cooled, the number density of DM particles decreased until they could not annihilate anymore, freezing out by the primordial thermodynamical equilibrium. Thenceforth their number density remained constant, fixed to the value observed today. This picture is described by a Boltzmann equation that, under certain assumptions, has the useful approximated solution [16]

$$\Omega_\eta h^2 \simeq \frac{3 \cdot 10^{-27} \mathrm{cm}^3 \mathrm{s}^{-1}}{\langle \sigma v_{\mathrm{rel}} \rangle} \,, \tag{3.1}$$

where $\Omega_\eta = \rho_\eta / \rho_c$ is the ratio between the energy density of DM and the critical energy density of the Universe, $h = H_0 / (100 \, \mathrm{km \, s^{-1} Mpc^{-1}})$ is the reduced value of the present Hubble parameter, and $\langle \sigma v_{\mathrm{rel}} \rangle$ is the thermal-average of the total annihilation cross section of DM particles, times their relative velocity. The present experimental value is $\Omega_{DM} h^2 = 0.1126 \pm 0.0036$ [17].[1]

Although the singlet pNGB η interacts strongly with the heavy resonances of the composite sector, its interactions with the SM, including the composite Higgs, are weak, as shown in eqs. (2.2)–(2.4); as a consequence, its annihilation cross section into fermions, gauge bosons and the Higgs falls into the ballpark suggested by eq. (3.1). In appendix B we display all the relevant annihilation cross-sections that enter in the Boltzmann equation, both in the non-composite and in the composite case. The Feynman rules needed in the computation are collected in table 2.

The numerical solution of the Boltzmann equation is shown in figure 1 as a function of m_η, for two representative values of λ. To understand the behavior of the relic density with m_η, one should keep in mind that each annihilation channel $\eta\eta \leftrightarrow X\bar{X}$ opens only for η masses above the threshold value $m_X \sqrt{1 - v_{\mathrm{rel}}^2/4}$, with $v_{\mathrm{rel}} \sim 2/3$ at freeze-out. In order to analyze the effect of the composite interactions, let us recall that in the non-composite

---

[1]An alternative mechanism to generate the DM relic density is freeze-in, that is realized when the DM interactions with the SM are so weak that the DM species was never in equilibrium. In this case SM particles can slowly annihilate (or decay) into DM generating the required relic density. For the case of a scalar singlet η coupled to the Higgs portal, freeze-in is possible both for m_η of the order of the electroweak scale [18] and for $m_\eta \lesssim 1 \, \mathrm{GeV}$ [19], as long as $\lambda \lesssim 10^{-10}$. Here we will consider only composite models that induce a larger value for λ as well as a large DM-Higgs derivative interaction. Therefore we will focus on the freeze-out scenario.
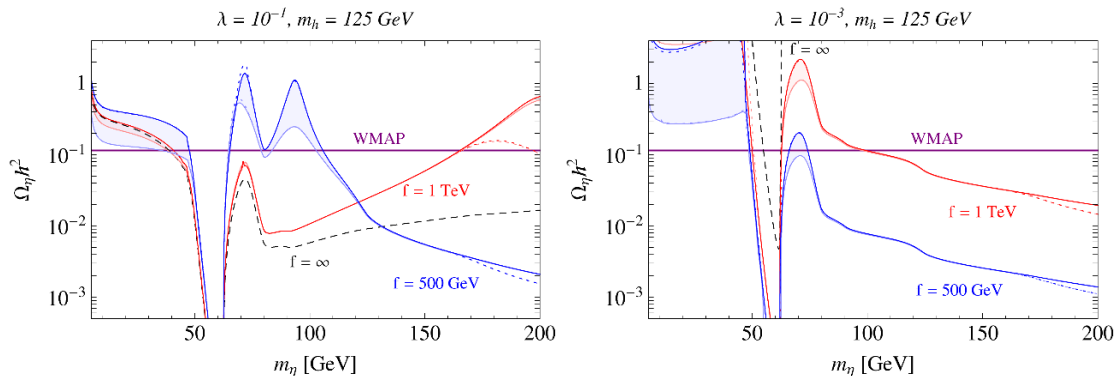
Figure 1. Relic density of the scalar singlet DM as a function of its mass m_η. We take $m_h = 125\,\text{GeV}$ and $\lambda = 10^{-1}$ (10^{-3}) in the left (right) panel. The dashed curves correspond to the non-composite case, the red (blue) curves to the composite case with $f = 1\,\text{TeV}$ $(500\,\text{GeV})$. The red and blue bands describe the variation of the DM−bottom coupling c_b in eq. (2.9), between $a = b = 0$ (dark lines) and $a = b = 1$ (light lines). Above the threshold for annihilation into $t\bar{t}$, the result depends also on the value of the DM−top coupling: the dotted and solid lines correspond to $c_t = 1/2$ (Case 1) and $c_t = 0$ (Case 2), respectively.

case the annihilation cross section is entirely determined by the value of λ (see eqs. (B.13)–(B.16)). In the composite case the situation is substantially different. One can identify four interesting mass regions:

1. *The low-mass region, $m_\eta \lesssim 50\,\text{GeV}$.* The annihilation cross-section is dominated by the $b\bar{b}$ channel, that is enhanced by the direct DM−bottom coupling proportional to c_b, shown in eq. (2.3). As a consequence, one can reproduce the DM relic density even for values of λ smaller than in the non-composite case.

2. *The resonant region, $m_\eta \simeq m_h/2$.* The presence of the Higgs resonance enhances the annihilation cross section by several orders of magnitude. In the non-composite case this is the only possibility to fit the DM relic density when λ is relatively small, however for too small values ($\lambda \lesssim 10^{-4}$ at $m_h = 125\,\text{GeV}$) even this enhancement is not sufficient and the model is excluded. On the contrary, in the composite case one can reproduce the DM relic density even for vanishing λ, because of the extra derivative contribution to the η-η-h vertex, coming from eq. (2.2).

3. *The cancellation region, $m_\eta^2 \sim \lambda f^2/2$.* A cancellation can occur between the derivative and the λ contributions to the η-η-h vertex (see eq. (2.2) and eq. (2.4), respectively), that may suppress the annihilation with s-channel Higgs-exchange when this is too large. The cancellation condition reads

$$s = 2\lambda f^2 (1 - \xi)\,, \tag{3.2}$$

where $s = 4m_\eta^2/(1 - v_{\text{rel}}^2/4)$. For example, for $\lambda = 10^{-1}$ and $f = 500\,\text{GeV}$, taking into account the freeze-out temperature one finds that the effect of the cancellation is maximal for $70\,\text{GeV} \lesssim m_\eta \lesssim 100\,\text{GeV}$, as one can see in the left panel of figure 1.

In the non-composite case ($f \to \infty$), when λ is sufficiently large the relic density is too suppressed for all values of m_η above the resonant region. In the case of compositeness, instead, the cancellation enhances the value of Ω_η and can make it compatible with the DM relic density. For larger f, the cancellation region moves out to larger values of m_η, where the $t\bar{t}$ channel opens. If the top has no direct coupling to η (solid lines in figure 1), the cancellation remains effective. If instead the top couples directly to DM (dotted lines), this reduces the relic density already for values of m_η in the cancellation region.

4. *The high-mass region.* As the DM mass increases, $m_\eta^2 \gg m_h^2/4$ and $m_\eta^2 \gg \lambda f^2/2$, the η-η-h vertex is more and more dominated by the derivative coupling of eq. (2.2), whose strength is uniquely fixed by f. As a consequence, the annihilation rate through the Higgs portal becomes larger (typically too large for $f = 500\,\text{GeV}$). Still, for $f \lesssim 1\,\text{TeV}$ the annihilation rate is of the correct order of magnitude, as can be seen in the right panel of figure 1. The proper relic density can be reproduced even for a vanishing λ.

The analysis of the η relic density will be completed in section 6, where we will show the contours for $\Omega_\eta = \Omega_{DM}$ in the plane (m_η, λ). Before that, we need to discuss the constraints coming from LHC Higgs searches (section 4), and from DM direct detection experiments (section 5).

4 Constraints from Higgs searches at the LHC

The SM Higgs boson mass was restricted to be heavier than $114\,\text{GeV}$ by LEP measurements. This limit applies also to a Higgs boson that decays invisibly, since even in this case the bound from associated production with a Z boson holds [20]. The LHC 95% C.L. upper bound in the low mass region is presently 127 (129) GeV from the CMS (ATLAS) experiment, assuming a SM-like Higgs. Here we will not discuss the very high mass region ($m_h \gtrsim 600\,\text{GeV}$) that is still allowed.[2] In the low mass region there is also a hint for a Higgs with $m_h \simeq 125\,\text{GeV}$, coming mostly from the decay channel $h \to \gamma\gamma$ ([21, 22]; see also the recent slides at http://indico.in2p3.fr/conferenceDisplay.py?confId=6001).

In the singlet extension of the SM, invisible Higgs decays are allowed as long as $m_h > 2m_\eta$. The observation of the Higgs boson would imply an upper bound on the invisible decay width, $\Gamma_{inv} \equiv \Gamma(h \to \eta\eta)$. Vice versa, a signal suppression could be explained by a sizable Γ_{inv}. In our scenario we find

$$\Gamma_{inv} = \frac{v^2}{32\pi m_h}\sqrt{1 - \frac{4m_\eta^2}{m_h^2}}\left(\frac{m_h^2}{v^2}\frac{\xi}{\sqrt{1-\xi}} - 2\lambda\sqrt{1-\xi}\right)^2 \vartheta(m_h - 2m_\eta)\,. \qquad (4.1)$$

In addition to the invisible decay channel, compositeness implies further deviations from the SM predictions, because the Higgs couplings to gauge bosons and fermions are modified at order ξ [15], as we will describe below. These modifications affect both the Higgs

---

[2]We have checked that, even for a very heavy Higgs boson, with $m_h \gtrsim 600\,\text{GeV}$, the composite singlet can still provide a good DM candidate.

production and the relative branching ratios for the Higgs decays into visible channels. Reduced (enhanced) couplings would weaken (strengthen) the Higgs signal at the LHC.

Let us discuss first the non-composite scenario, when ξ vanishes. In this case the LHC exclusion limits on the Higgs mass are conveniently described by the ratio

$$\mu \equiv \frac{\sigma(pp \to h \to SM)}{\sigma_{\rm SM}(pp \to h \to SM)} \equiv \frac{\sigma(pp \to h)}{\sigma_{\rm SM}(pp \to h)} BR(h \to SM) = \frac{\Gamma_{\rm SM}}{\Gamma_{\rm SM} + \Gamma_{inv}} , \qquad (4.2)$$

where $\Gamma_{\rm SM}$ is the total Higgs width in the SM, and Γ_{inv} is given by eq. (4.1) in the limit $\xi \to 0$. Note that the Higgs production cross section is unchanged w.r.t. the SM, however the Higgs visible branching ratio becomes smaller than one, as long as $m_h > 2m_\eta$. Actually for $|\lambda| \gtrsim 0.1$ the channel $h \to \eta\eta$ dominates.

In the case of composite h and η, there are several important differences. First, there is another $h-\eta-\eta$ coupling besides λ, that arises from the derivative interaction in eq. (2.2). As a consequence, the two contributions to the decay amplitude in eq. (4.1) can cancel each other for $\lambda > 0$, or add up for $\lambda < 0$. In the former case the Higgs signal at the LHC is maximal for $\lambda \simeq m_h^2/2f^2$, rather than for $\lambda = 0$.

Second, as we mentioned, there are order ξ modifications of the Higgs couplings, that are specific to the composite nature of h independently from the existence of a light singlet η. For concreteness, we will center here on the SO(6)/SO(5) models described in appendix A, assuming Case 2 for the top quark. The relevant Higgs couplings are modified as follows:

$$g_{hVV} = g_{hVV}^{\rm SM}\sqrt{1-\xi} \quad \text{for } V = W, Z, \qquad (4.3)$$

$$g_{ht\bar{t}} = g_{ht\bar{t}}^{\rm SM}\sqrt{1-\xi} , \qquad (4.4)$$

$$g_{hb\bar{b}} = g_{hb\bar{b}}^{\rm SM}\frac{1-2\xi}{\sqrt{1-\xi}} . \qquad (4.5)$$

The Higgs coupling to gluons, which is crucial for the total production cross section, is mainly generated by top loops involving the coupling $g_{ht\bar{t}}$ linearly. Therefore we have[3]

$$g_{hgg} \simeq g_{hgg}^{\rm SM}\frac{g_{ht\bar{t}}}{g_{ht\bar{t}}^{\rm SM}} = g_{hgg}^{\rm SM}\sqrt{1-\xi} . \qquad (4.6)$$

Similarly to the case of gluons, the Higgs coupling to photons is dominated by a top quark loop and a W-loop, that involve linearly $g_{ht\bar{t}}$ and g_{hWW} respectively. Since both couplings are corrected in the same way (see eqs. (4.3) and (4.4)), one finds

$$g_{h\gamma\gamma} \simeq g_{h\gamma\gamma}^{\rm SM}\sqrt{1-\xi} . \qquad (4.7)$$

In order to compare these effects of compositeness with the LHC results, one should notice that the most sensitive channels in the present analyses by ATLAS and CMS are $h \to \gamma\gamma, WW, ZZ$. Therefore, what is actually measured is not the total Higgs signal

---

[3]One should remark that, in composite Higgs model, the suppression of the top quark contribution to g_{hgg} could be compensated by the contributions of heavier states, such as vector-like fermions that accompany the top, or other resonances of the strongly-interacting sector. However, in most cases it was found that no enhancement of the Higgs production occurs, but exceptions are possible [23–25].
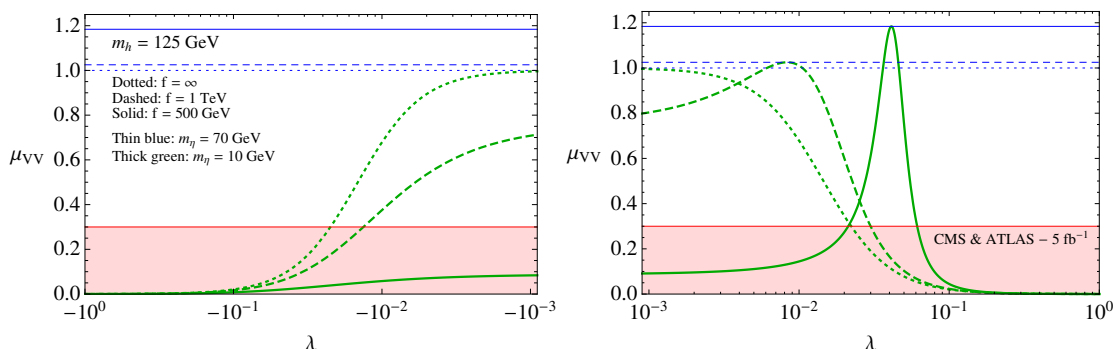
Figure 2. The strength μ_{VV} of the Higgs signal in the gauge channels, defined in eq. (4.8), as a function of the $h - \eta$ quartic coupling λ (negative in the left panel, positive in the right panel). We chose $m_h = 125\,\text{GeV}$ and two values for the scalar singlet mass m_η, one larger than $m_h/2$ and the other smaller. The dotted curves correspond to the non-composite case. The dashed (solid) curves correspond to compositeness with $f = 1\,\text{TeV}$ (500 GeV). We took into account the order ξ corrections to the Higgs couplings to vector bosons and fermions, see eqs. (4.3)–(4.7). The shaded region is disfavoured by the LHC Higgs searches (we roughly extracted the 95% C.L. lower bound on μ_{VV} from ref. [21, 22]).

strength μ, rather the signal strength in the 'gauge' decay channels only. As a consequence, the relevant quantity is

$$\mu_{VV} \equiv \frac{\sigma(pp \to h \to VV)}{\sigma_{\text{SM}}(pp \to h \to VV)} \equiv \frac{\sigma(pp \to h)}{\sigma_{\text{SM}}(pp \to h)} \frac{\Gamma(h \to VV)}{\Gamma_{\text{SM}}(h \to VV)} \frac{\Gamma_{\text{SM}}}{\Gamma_{\text{SM}}^{\text{comp}} + \Gamma_{inv}}$$

$$\simeq (1-\xi)(1-\xi) \frac{\Gamma_{\text{SM}}^{\psi\bar\psi} + \Gamma_{\text{SM}}^{VV}}{\Gamma_{\text{SM}}^{\psi\bar\psi}(1-2\xi)^2/(1-\xi) + \Gamma_{\text{SM}}^{VV}(1-\xi) + \Gamma_{inv}}, \tag{4.8}$$

where $V = \gamma, Z, W$, and we assumed that the Higgs production is dominated by the gluon fusion channel, controlled by eq. (4.6). Here $\Gamma_{\text{SM}}^{\text{comp}}$ is the total visible width in the composite scenario, while $\Gamma_{\text{SM}}^{\psi\bar\psi}$ and Γ_{SM}^{VV} are the total SM widths into fermions and gauge bosons, respectively. Note that, in the non-composite case, eq. (4.8) reduces to eq. (4.2).

In figures 2, 3 we display our prediction for μ_{VV} as a function of λ. Since the gauge channels are the most sensitive at the LHC, the experimental constraints on μ [21, 22] are more appropriately interpreted as constraints on μ_{VV}. The red shaded regions in figures 2, 3 are disfavoured at 95% C.L.. Let us discuss the 'light' and 'heavy' Higgs scenarios in turn.

SM-like Higgs with $m_h \lesssim 130\,\text{GeV}$. (Figure 2) If the signal around $m_h = 125\,\text{GeV}$ were confirmed, the ratio μ_{VV} should lie relatively close to one. More precisely, the CMS (ATLAS) collaboration finds the largest excess at $m_h = 124(126)\,\text{GeV}$, with $\mu_{VV} = 0.6 - 1.2\ (0.6 - 1.3)$ at 1σ [21, 22]. Given this large statistical uncertainty, in figure 2 we roughly estimated the 95% C.L. lower bound as $\mu \gtrsim 0.3$.

In the non-composite case, for $m_\eta > m_h/2$ one has $\mu_{VV} = 1$, while for $m_\eta < m_h/2$, in order to avoid a too large Γ_{inv}, one is forced to take sufficiently small values of λ.

In the composite case instead, when $m_\eta > m_h/2$ we find that μ_{VV} can be larger than one. Indeed eq. (4.8) shows that, even though the Higgs production is suppressed by a
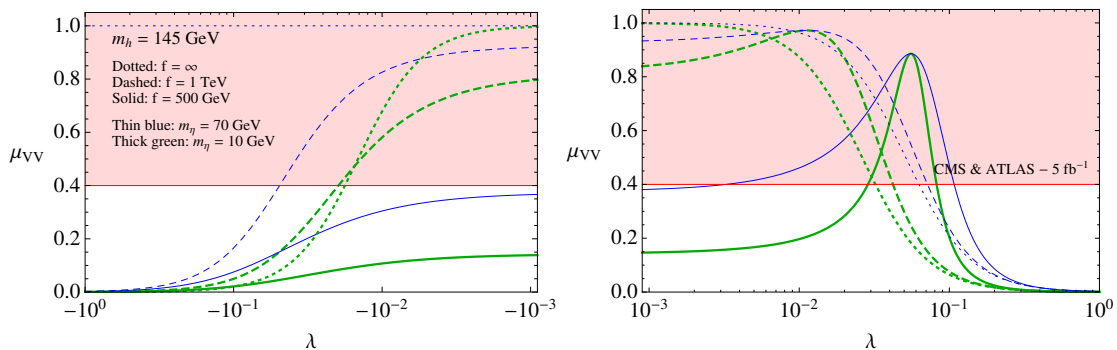
Figure 3. The same as in figure 2, except for $m_h = 145\,\text{GeV}$. For this mass ATLAS and CMS put an upper bound on μ_{VV}.

factor $(1-\xi)$, the gauge decay channels receive a $(1-\xi)^2/(1-2\xi)^2$ enhancement relatively to the fermion channels (which dominate the branching ratio up to $m_h \simeq 135\,\text{GeV}$). As a consequence, one finds that μ_{VV} can be as large as 1.2 for f as small as $500\,\text{GeV}$. When $m_\eta < m_h/2$, the signal is suppressed by Γ_{inv}. However larger values of λ are allowed w.r.t. the non-composite case, as shown in the right panel of figure 2, because of the cancellation between the two terms in brackets in eq. (4.1).

Invisible Higgs with $m_h \gtrsim 130\,\text{GeV}$. (Figure 3) In this region the LHC searches exclude a SM-like Higgs, by requiring the ratio μ_{VV} to be smaller than one. In our scenario, this can be accounted for by the combined effect of invisible decays and reduced SM couplings, as illustrated in figure 3, where we fix $m_h = 145\,\text{GeV}$ (for this value of the Higgs mass the most sensitive channels are $h \to WW \to 2l2\nu$ and $h \to ZZ \to 4l$). In this case the 95% C.L. upper bound from ATLAS and CMS is roughly $\mu_{VV} \lesssim 0.4$. There are wide regions of parameter space that survive the LHC constraint, as shown by the curves lying in the unshaded region in figure 3.

5 Constraints from dark matter searches

The direct detection of DM is based on the observation of the elastic scattering between non-relativistic DM particles from our galaxy halo and cryogenic nuclei in targets, that produces a nuclear recoil. In our scenario the interaction of the composite DM η with nucleons arises through the direct couplings c_q ($q = u, d, \dots$) between DM and quarks, given in eq. (2.3), and through the t-channel exchange of a Higgs boson, which in turn couples with quarks; in both cases heavy quark loops also induce a coupling to the gluons in the nucleons. These processes give rise to a spin-independent elastic cross section σ_{SI}, potentially within the reach of present and future experiments. Note that $\text{Im}(c_q)$ contributes only to the spin-dependent cross-section σ_{SD}, which is always much smaller than σ_{SI} (the latter being enhanced by the coherent interactions on protons and neutrons in the large target nucleus).

The XENON100 experiment recently set the best experimental upper limit on σ_{SI} [26], and it plans to considerably improve its sensitivity already within the end of 2012. The
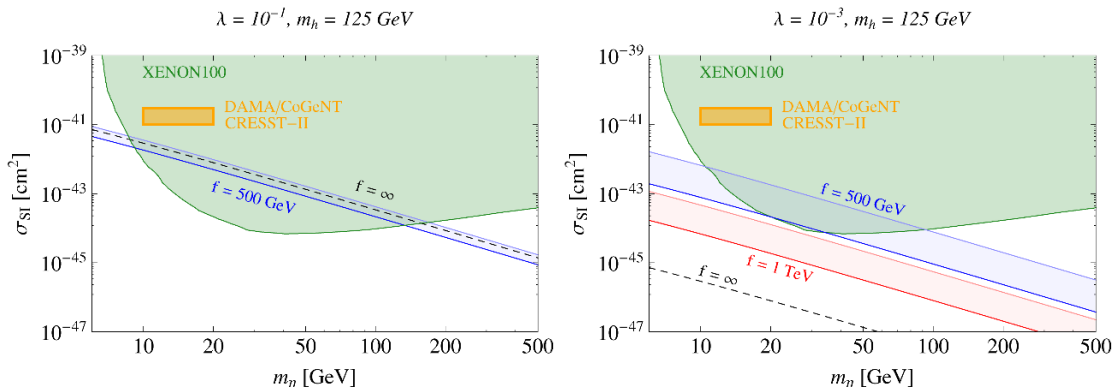
Figure 4. The spin-independent cross section for the elastic scattering of the DM candidate η off nuclei. The green shaded region is excluded by XENON100 [26], while the orange shaded region roughly corresponds to the excess events reported by DAMA, CoGeNT and CRESST-II [32, 33]. The predictions of our scenario are labeled in the same way as in figure 1. The two panels correspond to two different values of λ, and we took Case 2 for the DM-quark couplings c_q. In the left panel, the band for $f = 1\,\mathrm{TeV}$ (not shown) is very similar to the one for $f = 500\,\mathrm{GeV}$.

excluded region at 90 % C.L. is shaded in green in figure 4. On the other hand, the DAMA/LIBRA collaboration (confirming previous results by DAMA/NaI) has provided the first evidence of an annual modulation in the event rate, that could be due to DM, with 8.9 standard deviations from the expected background [27, 28]. Similar signals have been observed by CoGeNT [29, 30] and by CRESST-II [31], which both measure an excess of low-energy nuclear recoil events. CoGeNT also observes a seasonal variation. The analysis performed e.g. in ref. [32, 33] shows that a DM candidate with $m_{DM} \simeq (10 - 20)\,\mathrm{GeV}$ and $\sigma_{\mathrm{SI}} \simeq (1 - 3) \cdot 10^{-41}$ cm^2 can account for the excess events reported by each of these experiments. This favoured region is shaded in orange in figure 4. One can appreciate the well-known tension between these signals and the exclusion limits of XENON100, that is presently unexplained.

In figure 4 we compare σ_{SI} in our scenario with the DM direct detection constraints, taking the same values of the parameters that we used for the relic density in figure 1. The calculation of σ_{SI} is a straightforward application of the standard formalism [34] to our composite scenario, that is defined by the effective interactions of η with quarks and gluons. The detailed equations are reported in appendix C, and can be summarized by the following estimate, which shows explicitly the relative size of the different contributions:

$$\sigma_{\mathrm{SI}} \simeq 3.5 \cdot 10^{-40} \mathrm{cm}^2 \left(\frac{10\,\mathrm{GeV}}{m_\eta} \right)^2 \left(\frac{125\,\mathrm{GeV}}{m_h} \right)^4 \tag{5.1}$$

$$\times \left[\lambda \left(1 - \frac{2v^2}{f^2} \right) + \frac{m_h^2}{f^2} \mathrm{Re} \left(0.04\,c_u + 0.11\,c_d + 0.18\,c_s + 0.22 \sum_{q=c,b,t} c_q \right) \right]^2 .$$

The first term in square brackets comes from Higgs-exchange, while the second term comes from the direct coupling between the DM and the light quarks and gluons (through a loop of heavy quarks) in the nucleon. Contrary to the relic density, the DM direct detection bounds are sensitive also to the couplings between η and the light quarks, mostly the

strange. The figure 4 shows σ_{SI} for the Case 2 defined in section 2: we vary $c_d = c_s = c_b$ in the range defined by eq. (2.9) and we take $c_{u,c,t} = 0$. Notice that the effect of the derivative coupling of eq. (2.2) is very small at low momentum transfer and it has been neglected.

For $\lambda = 10^{-1}$ (left panel of figure 4), the first term of eq. (5.1) dominates and σ_{SI} is of the same order of magnitude as in the non-composite case. By comparing with figure 1, one remarks that the correct relic density can be reproduced by $m_\eta \sim 10\,\text{GeV}$, with a DM candidate that lies close to the region preferred by DAMA, CoGeNT and CRESST-II, or by $m_\eta \sim 80\,\text{GeV}$, in a region already excluded by XENON100, or by $m_\eta > 150\,\text{GeV}$, with no constraints from present direct detection bounds. For $\lambda = 10^{-3}$ (right panel of figure 4), the difference w.r.t. the non-composite case is more important. The correct relic density is reproduced e.g. for $f = 1\,\text{TeV}$ and $m_\eta \simeq 100\,\text{GeV}$ (see figure 1). This candidate is compatible with the present XENON100 bound, and it is within the reach of near future measurements with improved sensitivity. For such small values of λ, on the contrary, the non-composite case cannot be probed in DM direct detection experiments.

We remark that the various contributions in eq. (5.1) can have opposite sign and (partially) compensate each other, reducing σ_{SI}. Above we assumed conservatively that all contributions are positive, but one cannot exclude a cancellation, e.g. switching to a negative value of λ. Therefore the DM direct detection bound is quite sensitive to the details of the theoretical model, and for specific values of the parameters our scenario can avoid this constraint.

Let us make now a few remarks about DM indirect detection experiments. Bounds from direct detection - as shown in figure 4 - allow for a light DM candidate with a mass $\lesssim 10\,\text{GeV}$. In this regime, the DM annihilation in the early Universe is entirely driven by the process $\eta\eta \leftrightarrow b\bar{b}$, with a required cross section of the order of $\langle\sigma v_{\text{rel}}\rangle \simeq 3{\cdot}10^{-26}\,\text{cm}^3\text{s}^{-1}$. This value weakly depends on the DM relative velocity, and therefore it remains constant from the freeze-out until today, resulting into a sizable antiproton flux on the earth, produced by the DM annihilation into quarks that hadronize. We estimated this flux using the tools in ref. [35, 36]. As already pointed out in ref. [37], this antiproton flux can be larger than the one observed by the PAMELA experiment [38], resulting in a constraint on the DM mass that is complementary to the direct detection one. One should keep in mind, however, the large astrophysical uncertainty of these observations, mainly due to the propagation of charged particles in the Galaxy. A mass m_η smaller than $10\,\text{GeV}$ is generically disfavoured, with the exact bound depending on the adopted propagation model. In addition, the DM annihilations can also leave a trace in the cosmic microwave background power spectra, the size of the effect being proportional to $\langle\sigma v_{\text{rel}}\rangle/m_\eta$. Assuming that $\langle\sigma v_{\text{rel}}\rangle$ is approximately velocity-independent, one finds that the Planck satellite should reach a sufficient sensitivity to observe such effect, as long as $m_\eta \lesssim 50\,\text{GeV}$ [39].

We remark also that when the DM annihilation process occurs close to the Higgs resonance, the Breit-Wigner enhancement mechanism is operative [40, 41], resulting in a large boost of the annihilation cross section today, w.r.t. its freeze-out value. This boost factor can be invoked to explain some recent anomalies reported in cosmic ray data [40, 42]. Notice that the same resonant enhancement may play a crucial role for the pair annihilation of DM particles into two, monochromatic high-energy gamma rays. This

channel is particularly relevant, given its peculiar spectral structure that cannot be confused with the continuum astrophysical backgrounds. A value of the DM mass too close to the Higgs resonance can exceed the upper limit ($\langle \sigma v_{\rm rel} \rangle_{\gamma\gamma} \sim 4 \cdot 10^{-28} {\rm cm}^3 {\rm s}^{-1}$ for $m_\eta \simeq 60\,{\rm GeV}$) recently established by the Fermi-LAT collaboration [43].

Finally, let us compare the DM direct detection bounds with those coming from collider searches of monojet plus missing transverse energy. Indeed, the singlet η might be pair-produced through its coupling to quarks; while the two singlets escape the detector, these events can be identified by the initial state radiation of a gluon or a photon. In some cases [44] these searches can provide comparable bounds to DM direct detection experiments, in particular for light fermionic DM (with $m_{DM} \lesssim 10\,{\rm GeV}$). This is however not the case for our composite singlet for three reasons. First, the reach of monojet searches is reduced for a light scalar DM than it is for a fermionic DM [45, 46]. Furthermore, in our scenario, the effective coupling of η to gluons depends on the momentum of the process (at the momenta involved in DM direct detection experiments, η couples more strongly to gluons than at collider energies), contrary to ref. [44] where the effective coupling was assumed to be constant. Finally, in our case bounds on the invisible Higgs decay (section 4) provide the strongest collider constraint. For these reasons we neglect bounds from monojet searches in what follows.

6 Combined results

We present in this section a combined analysis of the parameter space for the composite singlet DM candidate η. The results are displayed in figures 5–7, in the plane (m_η, λ). We require to reproduce the observed value of the DM relic density (the purple contour corresponds to $\Omega_\eta = \Omega_{DM}$), and we take into account DM direct detection experiments (the green region is disfavoured by XENON100) and Higgs searches (the red region is disfavoured by ATLAS and CMS).

$m_h = 125\,{\rm GeV}$, $f = 500\,{\rm GeV}$: a DM candidate with $m_\eta \simeq 70\,{\rm GeV}$. We begin by taking the Higgs mass value presently preferred at the LHC, $m_h = 125\,{\rm GeV}$, and choosing the characteristic pNGB scale close to the lower bound coming from electroweak precision tests, $f = 500\,{\rm GeV}$. We focus on Case 2 (a vanishing coupling c_t between the top quark and the DM), since it allows for a light η, $m_\eta \lesssim m_h$. This scenario is illustrated in figure 5.

In the non-composite case ($f = \infty$, dashed contours), a viable DM candidate lies in correspondence to the Higgs resonance ($m_\eta \simeq 60\,{\rm GeV}$, $\lambda \lesssim 0.02$), or beyond the kinematical threshold for annihilation into electroweak gauge bosons ($m_\eta \gtrsim 80\,{\rm GeV}$, $\lambda \simeq 0.04$).

In the composite case the situation changes considerably. Note first that the region $m_\eta \lesssim m_h/2$ is disfavoured by the LHC Higgs signal excess, because the Higgs decay width is dominated by the hidden decay channel into DM, except for $\lambda \simeq m_h^2/(2f^2) \simeq 0.03$, where a cancellation in Γ_{inv} takes place. Note also that the direct detection bound is strengthened by the composite interactions, because of the contribution of direct DM−quark couplings, see eq. (5.1).

Taking into account these constraints, a definite prediction follows from figure 5: $m_\eta \simeq 70\,{\rm GeV}$ with $\lambda \lesssim 0.02$. At small values of λ, the η-η-h vertex is dominated by the derivative
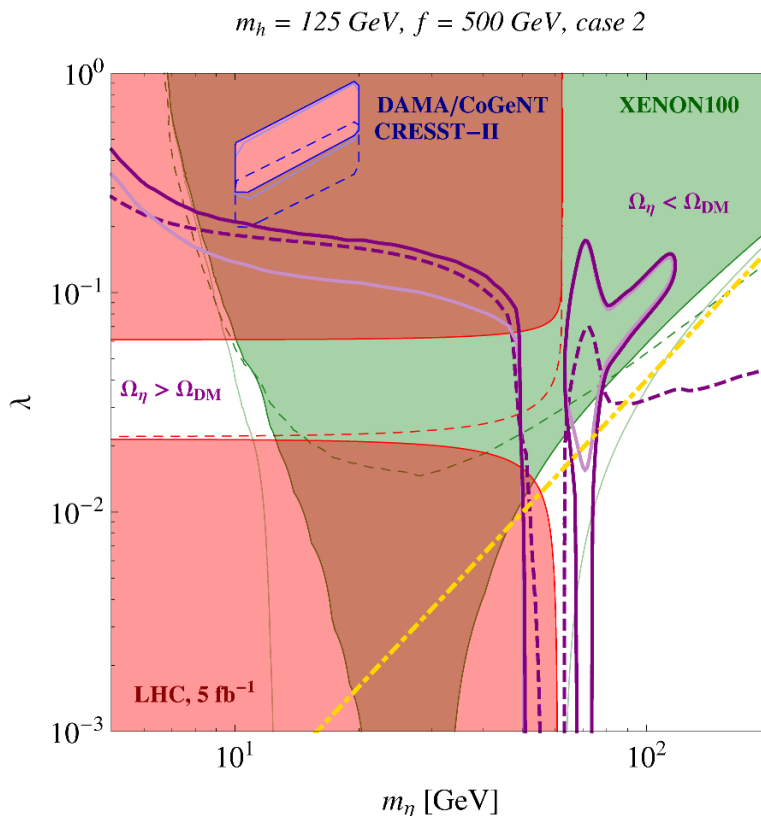
Figure 5. The contour $\Omega_\eta = \Omega_{DM}$ (solid dark purple line) in the plane (m_η, λ), for $m_h = 125\,\text{GeV}$, $f = 500\,\text{GeV}$, assuming Case 2 with $c_b = 1/2$. The green shaded region is disfavoured by XENON100, the region delimited by a blue line is favoured by DAMA/CoGeNT/CRESST-II, and the red shaded region is disfavoured by the Higgs signal at the LHC. The solid light purple/green/blue lines correspond to the same observables for maximal c_b ($a = b = 1$ in eq. (2.9)). The dashed purple/green/blue/red lines correspond to the same observables in the non-composite case, $f = \infty$. Finally, the region below the yellow dot-dashed line corresponds to the theoretical preferred region defined by eq. (2.6).

coupling, therefore the relic density becomes independent from λ and the purple lines in figure 5 become vertical. For higher DM masses the derivative interaction becomes too strong to accommodate the relic density (unless one enters in the "cancellation region", at relatively large values of λ, which is however excluded by XENON100).

One may ask if the region of parameters that is allowed phenomenologically is also compatible with the theoretical expectations. Independently of the specific model, we expect from eq. (2.6) that $m_\eta^2 \gtrsim \lambda f^2$. The region satisfying this relation lies below the yellow dot-dashed line in figure 5, and it is compatible with the phenomenologically preferred region.

$m_h = 125\,\text{GeV}$, $f = 1\,\text{TeV}$: DM candidates with $m_\eta \simeq 60\,\text{GeV}$ and $100 \lesssim m_\eta \lesssim 500\,\text{GeV}$. As the scale f increases, the composite interactions become weaker, and the bounds from the LHC Higgs signal and from XENON100 become less stringent and closer to the non-composite case. This is illustrated in figure 6, where we take $f = 1\,\text{TeV}$. In particular, all values of m_η are viable for $\lambda \lesssim 10^{-2}$.
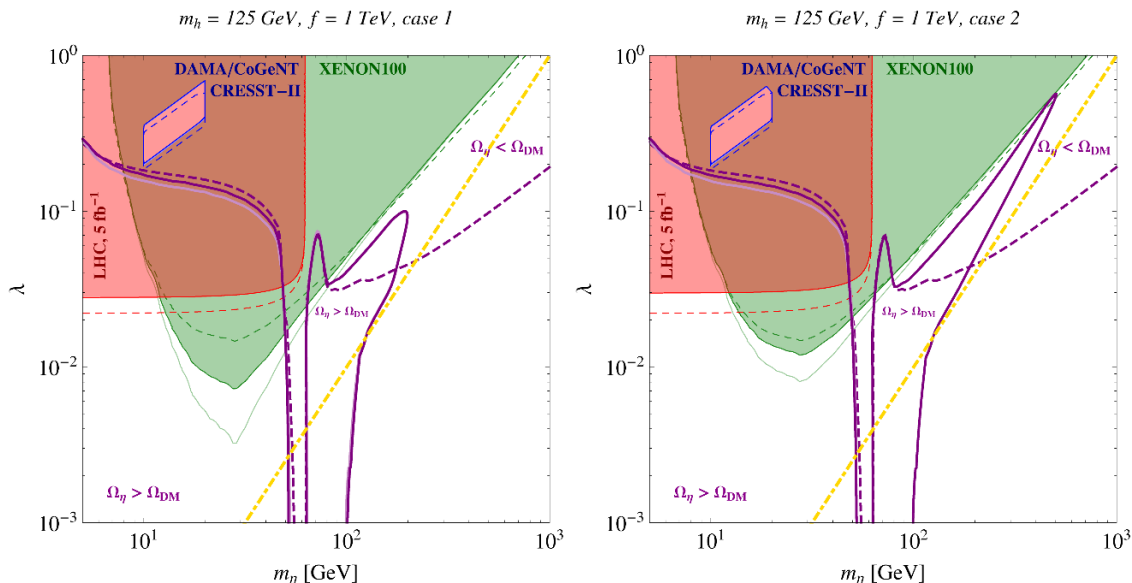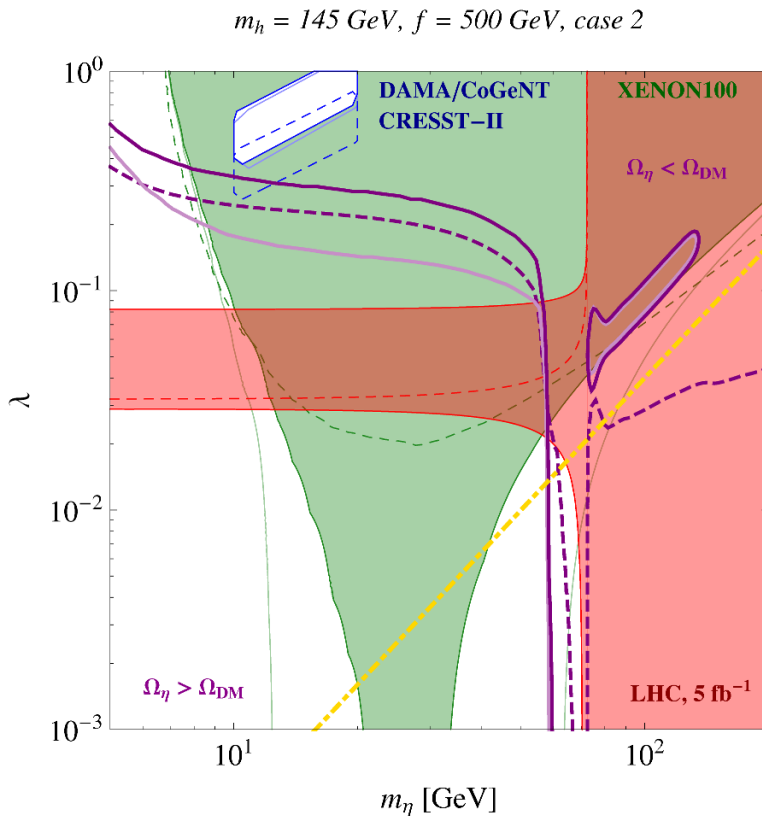
Figure 6. The same as in figure 5, but with $f = 1\,\text{TeV}$ and with a comparison between two scenarios for the top quark couplings: Case 1 (left panel) and Case 2 (right panel), as defined at the end of section 2.

The correct DM relic density can be accommodated for m_η lying a bit below or above the Higgs resonance at $m_h/2 \sim 60\,\text{GeV}$, or for $m_\eta \gtrsim 100\,\text{GeV}$, where the derivative interaction η-η-h in eq. (2.2) becomes of the right order to give the correct annihilation cross-section above the WW threshold. Furthermore, for relatively large values of λ, one enters in the cancellation region described in section 3: the DM annihilation is suppressed and the relic density can be accommodated even for very large values of the DM mass, up to $m_\eta \simeq 500\,\text{GeV}$ in Case 2 (right panel of figure 6). If the annihilation into $t\bar{t}$ is stronger (Case 1, left panel of figure 6), the allowed region closes earlier, at $m_\eta \simeq 200\,\text{GeV}$.

As discussed above, composite models prefer $\lambda \lesssim m_\eta^2/f^2$ (the region below the yellow dot-dashed line) that is compatible with the Higgs-resonance region for $\lambda \lesssim 0.003$, and with the region dominated by the derivative coupling, for $\lambda \lesssim 0.02$. On the contrary, the cancellation region is slightly disfavoured theoretically, even though λ larger by a factor of a few is sufficient to realize the cancellation.

$m_h = 145\,\text{GeV}$, $f = 500\,\text{GeV}$: DM candidate with $m_\eta \lesssim 10 - 20\,\text{GeV}$ and $m_\eta \simeq 60\,\text{GeV}$. In case the LHC excess at $125\,\text{GeV}$ were not confirmed, the Higgs boson might be heavier, as long as it decays invisibly with a sufficient rate to avoid the LHC bound. In order to illustrate this possibility, in figure 7 we choose a representative value $m_h = 145\,\text{GeV}$, assuming for definiteness $f = 500\,\text{GeV}$ and Case 2 (the results are very similar in Case 1).

The LHC bound is satisfied easily below the kinematical threshold for Higgs decays into DM, $m_\eta < m_h/2$, in a region of parameters which is very much complementary to the one allowed in figure 5. As a consequence, a light DM candidate with a mass $m_\eta \lesssim 10\,\text{GeV}$ is compatible with XENON100 and LHC. A light singlet with $10\,\text{GeV} \lesssim m_\eta \lesssim 20\,\text{GeV}$

$m_h = 145\,GeV,\ f = 500\,GeV,\ case\ 2$

Figure 7. The same as in figure 5, but with $m_h = 145\,\text{GeV}$.

could in principle explain the DAMA/CoGeNT/CRESST-II results (of course, in tension with the XENON100 bound). However the value $\lambda \lesssim 0.3$ required by the relic density is slightly smaller than the one needed to fit the signal in these experiments: for larger λ, η accounts only for part of the DM relic density.

In any case, the large coupling $\lambda \gtrsim 0.1$, needed to explain the relic density when $m_\eta \lesssim 20\,\text{GeV}$, is in contradiction with theoretical expectations. Indeed, the singlet receives at least a contribution to its mass-squared of order $\lambda v^2 \gtrsim (80\,\text{GeV})^2$, and the NDA expectation is actually much larger, $m_\eta^2 \gtrsim \lambda f^2 \gtrsim (160\,\text{GeV})^2$. Therefore, the case of a light singlet is disfavoured in the context of composite models, since it requires a large cancellation between different contributions to the singlet mass.

The other viable DM candidate in figure 7 lies just before the Higgs resonance, at $m_\eta \simeq 60\,\text{GeV}$, as long as $\lambda \lesssim 0.02$. This solution lies in the theoretically favoured region, and it requires a not too large $\text{Re}(c_b)$, in order to avoid the XENON100 bound.

In summary, it is interesting that the composite scalar DM model is very predictive, despite the new non-renormalizable interactions, generated by the strong sector at the TeV scale. In some cases, the composite singlet DM is even more constrained than the non-composite one. Indeed, in good approximation, the relic density and the LHC bounds depend only on m_η, λ and the derivative interaction between η and the Higgs, whose strength is uniquely fixed by the pNGB scale f. Therefore, our results are independent

from the specific composite model, up to the relatively small modifications due to the choice of the parameters c_t (compare the two panels in figure 6) and c_b (compare the dark and light contours in figures 5–7). The largest model-dependence lies in the DM direct detection bound for small values of λ. The most interesting DM candidates (for $m_h = 125\,\text{GeV}$) have mass $m_\eta \simeq 60 - 70\,\text{GeV}$, around the Higgs resonance, or lie in the region $100\,\text{GeV} \lesssim m_\eta \lesssim 200\,\text{GeV}$. In both cases small values of the Higgs portal coupling, $\lambda \lesssim 0.03$, are favored both phenomenologically and theoretically.

7 Conclusions and prospects

We have studied the phenomenology of a composite DM candidate, arising from the $O(6)/O(5)$ global symmetry breaking pattern. The light scalar spectrum of this model is formed by five pNGBs, which correspond to the Higgs doublet H and the real singlet η, that plays the role of the DM. They are lighter than the dynamically-generated scale $m_\rho \sim \text{TeV}$, due to their pNGB nature. We have shown that the DM phenomenology is strongly affected by the composite nature of the pNGBs, that allows for

(i) derivative interactions between η and H which grow as p^2/f^2, where p is the relevant momentum;

(ii) contact interactions c_ψ between η and the SM fermions ψ that break the η-shift symmetry and are suppressed by $m_\psi p/f^2$;

(iii) modification of the Higgs couplings to gauge bosons and fermions at order v^2/f^2.

We found that this scenario is very predictive, and it is actually easier to test than the non-composite case, which depends only on the Higgs portal interaction λ.

The most important phenomenological consequences of the properties (i)-(iii) are the following. The η annihilation cross section grows with m_η because of the derivative interaction between H and η. Therefore, to reproduce the DM relic density, one needs $m_\eta \lesssim 500\,\text{GeV}$ (for $f \lesssim 1\,\text{TeV}$). The same derivative interaction implies that the invisible Higgs decay in two DM particles is possible even for vanishing λ. On the other hand, the composite Higgs can be slightly fermiophobic and privilege decays into gauge bosons, as preferred by recent LHC data. The couplings c_ψ can significantly increase the DM scattering cross-section on nuclei: a signal in DM direct detection experiments is possible even for vanishing λ, as long as $10\,\text{GeV} \lesssim m_\eta \lesssim 100\,\text{GeV}$ and $f \lesssim 1\,\text{TeV}$.

Once all the constraints are taken into account, we are left with only three regions of parameters for our DM candidate:

1. Light mass region, with $m_\eta \simeq 10 - 20\,\text{GeV}$, close to the values preferred by the signals of DAMA/CoGeNT/CRESST-II. In this case the Higgs has a substantial invisible width into DM, that would be strongly disfavoured if the LHC hint for $m_h \simeq 125\,\text{GeV}$ were confirmed. Such light DM also contrasts with the theoretical expectations, because it requires a large coupling $\lambda \gtrsim 0.1$, and therefore a strong cancellation is needed to make the DM mass small.

2. Intermediate mass region, with $m_\eta \simeq 50-70\,\mathrm{GeV}$, where η annihilates mostly through the Higgs resonance. This region of parameters is almost the same as in the non-composite case, but a discrimination is possible for $f \sim 500\,\mathrm{GeV}$, where the LHC and DM direct detection constraints are significantly different. For $m_\eta < m_h/2$, Higgs invisible decays are expected, resulting in a reduction of the LHC Higgs signal.

3. Heavy mass region, with $m_\eta \simeq 100-500\,\mathrm{GeV}$, in which the annihilation cross-section is dominated by the derivative interaction between H and η. The latter is fixed by the value of f, and the relic density is actually too small for $f \sim 500\,\mathrm{GeV}$, but it becomes the correct one when $f \sim 1\,\mathrm{TeV}$. This case is possibly the most interesting, since the relevant DM interactions are completely determined by its composite nature, and it can be tested in near future DM direct searches (in contrast to the non-composite case). Moreover a DM mass close to the Higgs mass would strongly suggest a common origin, that is to say, both are generated radiatively by order one couplings to the top quark.

Other indirect signals of our scenario are the following. Since the Higgs is also composite, its couplings to the SM particle differ from an ordinary Higgs, as it can be explicitly seen in eqs. (4.3)–(4.7). It has been shown in refs. [15, 47–50] that the LHC with greater integrated luminosity could discriminate between standard and composite Higgs for values of $f \sim 500\,\mathrm{GeV}$. Furthermore, the Higgs can decay into two η that could be measured as an invisible decay width, as long as η is sufficiently lighter than the Higgs. When η is heavier, at large center-of-mass energy searches for monojets plus missing transverse energy might be the most sensitive to the derivative coupling, and they deserve further investigation. Also, heavy resonances ρ of the strong sector could decay into the DM with a sizable branching ratio for large g_ρ. For example, the decay $\rho \to \eta\eta W$ could result in a distinctive signal with leptons and large missing energy in the final state.

Let us briefly comment on another cosmological implication of a singlet scalar. It has been pointed out [51, 52] that a real singlet with the parity of eq. (2.1) can help in inducing a strongly first order electroweak phase transition, and thus play an important role in electroweak baryogenesis, as well as leave an observable spectrum of gravitational waves [53]. It would be interesting to check whether this possibility can be realized together with the singlet being DM. Although it seems unrealistic for an elementary singlet (the couplings needed to fit the relic density are too small to play a role during the phase transition), it could be possible for a composite η, that has large additional interactions.

In summary, we have presented a minimal composite framework that accounts for the Higgs boson and for a scalar DM in a natural way. Future DM searches (e.g. XENON1T) and LHC measurements shall be able to close on the three most promising regions of parameters described above, and thus establish or refute the connection between the EWSB sector and the DM sector.

A   The composite $O(6)/O(5)$ model for dark matter

In this appendix we present a model of a composite sector that accommodates the Higgs doublet H and the DM singlet η as pNGBs. The analysis is intended to provide the reader with a concrete realization of the effective lagrangian that we used all over our phenomenological study, and to compute the expected values of the pNGBs masses and couplings. The coset SO(6)/SO(5) provides the minimal realization of a set of pNGBs with the quantum numbers of H and η. This coset was first studied in ref. [10], with focus on the modifications of the Higgs phenomenology in the presence of a real scalar singlet. Here we demand that η plays the role of DM particle and we derive its properties, under the requirement of a consistent EWSB.

We assume a strong sector, with a mass gap $m_\rho \sim \text{TeV}$, whose global symmetry breaking pattern is SO(6) → SO(5). This can be achieved by a composite field Σ in the fundamental representation $\mathbf{6}$ of SO(6), that acquires a VEV

$$\Sigma_0 = (0, 0, 0, 0, 0, 1)^T . \tag{A.1}$$

The five NGBs transform as a $\mathbf{5}$ of SO(5), which decomposes as $\mathbf{4} \oplus \mathbf{1} \simeq (\mathbf{2}, \mathbf{2}) \oplus (\mathbf{1}, \mathbf{1})$ under the subgroup SO(4) $\simeq$ SU(2)$_L \times$ SU(2)$_R$. The NGBs describe the fluctuations along the broken directions, whose generators can be written as

$$T_{ij}^{\hat{a}} = -\frac{i}{\sqrt{2}} \left(\delta_i^{\hat{a}} \delta_j^6 - \delta_j^{\hat{a}} \delta_i^6 \right), \quad \hat{a} = 1, \ldots, 5. \tag{A.2}$$

The SO(6)/SO(5) coset is parametrized by

$$\Sigma = \exp\left(i \frac{\sqrt{2} \pi^{\hat{a}} T^{\hat{a}}}{f} \right) \Sigma_0 = \sin\frac{\pi}{f} \left(\frac{\tilde{h}_1}{\pi}, \ \frac{\tilde{h}_2}{\pi}, \ \frac{\tilde{h}_3}{\pi}, \ \frac{\tilde{h}_4}{\pi}, \ \frac{\tilde{\eta}}{\pi}, \ \cot\frac{\pi}{f} \right)^T$$

$$= \left(h_1, \ h_2, \ h_3, \ h_4, \ \eta, \ \sqrt{1 - h^2 - \eta^2} \right), \tag{A.3}$$

with $\pi^{\hat{a}} \equiv (\tilde{h}_i, \tilde{\eta})$, $\pi \equiv \sqrt{\sum_{i=1}^4 \tilde{h}_i^2 + \tilde{\eta}^2}$, and a field redefinition

$$h_i \equiv \frac{\tilde{h}_i}{\pi} \sin\frac{\pi}{f}, \qquad \eta \equiv \frac{\tilde{\eta}}{\pi} \sin\frac{\pi}{f}, \tag{A.4}$$

with $h^2 \equiv \sum_{i=1}^{4} h_i^2$. The usual Higgs doublet is given by $H = f[(h_1 + ih_2)/\sqrt{2},\ (h_3 + ih_4)/\sqrt{2}]$. In the unitary gauge three NGBs are eaten by the weak gauge bosons, and one is left with the Higgs boson $h \equiv h_3$ and η.

The NGB chiral lagrangian reads, up to terms with four derivatives,

$$\mathcal{L}_{kin} = \frac{f^2}{2}|D_\mu \Sigma|^2 = \frac{f^2}{2}\left[(\partial_\mu h)^2 + (\partial_\mu \eta)^2 + \frac{(h\partial_\mu h + \eta\partial_\mu \eta)^2}{1 - h^2 - \eta^2}\right.$$
$$\left. + \frac{g^2 h^2}{2}\left(W^{\mu+}W_\mu^- + \frac{1}{2\cos^2\theta_W}Z^\mu Z_\mu\right)\right]. \qquad (A.5)$$

From the last term in eq. (A.5), it is clear that the scale of EWSB is set by the VEV of h: $\langle h \rangle \equiv v/f = \sqrt{\xi}$. Note that $\mathcal{L}_{kin}$ is symmetric under the parity $P_\eta : \ \eta \to -\eta$, but higher derivative terms in the $SO(6)/SO(5)$ chiral lagrangian, involving the Levi-Civita tensor (such as the Wess-Zumino-Witten term [10]), are not. Since P_η is crucial to make η stable and thus a viable DM candidate, we need to assume that it is a symmetry of the whole composite sector and it is not spontaneously broken. This amounts to take the global symmetry breaking pattern to be $O(6) \to O(5)$, with

$$P_\eta = \text{diag}(1, 1, 1, 1, -1, 1), \qquad (A.6)$$

and to require $\langle \eta \rangle = 0$. Note also that, once h acquires a VEV, its kinetic term receives a correction from the third term in the square bracket of eq. (A.5). The physical Higgs and DM bosons (with a canonical kinetic term) are defined as follows:

$$\frac{h_{phys}}{f} = \frac{h - \langle h \rangle}{\sqrt{1 - \xi}}, \qquad \frac{\eta_{phys}}{f} = \eta. \qquad (A.7)$$

In all the observables we studied, we consistently used the couplings of the physical fields (but dropping the subscript '$phys$' everywhere).

The EWSB is triggered by the couplings of the SM gauge bosons and fermions to the composite sector, that break $O(6)$ explicitly, generating an effective potential for the pNGBs at the one-loop level. Still, we will show that under some conditions P_η is preserved by the gauge and fermion interactions as well. In this case, the most general form of the effective potential for h and η can be written as

$$V_{\text{eff}}(h, \eta) = \frac{f^2}{2}\left(\mu_h^2 h^2 + \mu_\eta^2 \eta^2\right) + \frac{f^4}{4}\left(\lambda_h h^4 + 2\lambda h^2 \eta^2 + \lambda_\eta \eta^4\right) + O((h, \eta)^6). \qquad (A.8)$$

Such potential must be minimized taking into account the constraint $h^2 + \eta^2 = \sin(\langle \pi \rangle /f) \leq 1$, that follows from eq. (A.4). We look for a minimum with $0 < h = v/f < 1$, to realize EWSB, and with $\eta = 0$, to preserve DM stability. The necessary and sufficient conditions for this to be a local minimum are $0 < -\mu_h^2 < f^2 \lambda_h$ and $\mu_\eta^2 \lambda_h > \mu_h^2 \lambda$, where we neglected the dimension-six terms in eq. (A.8).[4] Then, the pNGB physical masses are given by

$$m_h^2 \simeq -2\mu_h^2 = 2\lambda_h v^2, \qquad m_\eta^2 \simeq \mu_\eta^2 + \lambda v^2, \qquad (A.9)$$

---

[4]The requirement for this to be the global minimum (in the region $h^2 + \eta^2 \leq 1$) involves some extra lengthy conditions, that are satisfied in a wide range of the potential parameters.

up to $O(\xi)$ corrections.

The size of the effective potential coefficients depends on the way the SM gauge bosons and fermions couple to the composite sector. Note that, in order to reproduce the hypercharge of the SM fermions, the global symmetry of the composite sector should be enlarged to $O(6) \times U(1)_X$, with the hypercharge defined by

$$Y \equiv T_R^3 + X . \tag{A.10}$$

Since η is a gauge singlet, its NGB nature is not affected by the gauging of $SU(2)_L \times U(1)_Y$, that is to say, it does not acquire a potential through the gauge loops. Therefore, the electroweak gauge bosons only contribute to the Higgs potential, inducing $\mu_h^2 \sim g^2 m_\rho^2/(16\pi^2)$ and $\lambda_h \sim g^4/(16\pi^2)$ (see ref. [10] for details). These contributions are generally smaller than those coming from the top quark, which will drive EWSB.

The eqs. (A.5), (A.7) and (A.8) define all the relevant interactions among η, h and the gauge bosons. The corresponding Feynman rules are displayed in table 2.

Coming to the SM fermion interactions with the strong sector, we assume the partial compositeness scenario [9, 54], which is preferred by the constraints on flavour violation: each SM chiral fermion ψ couples linearly to a composite operator $\mathcal{O}_\psi$ of the strong sector:

$$\mathcal{L}_{\text{int}} = \lambda_\psi \overline{\psi}\, \mathcal{O}_\psi + h.c.. \tag{A.11}$$

This leads to a mixing of the SM fermions with the heavy composite states (of mass $\sim m_\rho$) of order λ_ψ/g_ρ. By repeating this reasoning for each SM chiral fermion, the Yukawa couplings turn out to be given by $y_\psi \simeq \lambda_{\psi_L}\lambda_{\psi_R}/g_\rho$.

Following standard techniques [9, 56], we will promote the SM fields ψ into spurions Ψ forming complete SO(6) representations. The Ψ are defined to transform as the SO(6)-multiplet $\mathcal{O}_\psi$ in such a way that the interaction eq. (A.11) can be written as an invariant under SO(6). The interactions between the SM fermions and the pNGBs h and η will crucially depend on the representation of Ψ under SO(6). We will identify the simplest representations that (i) allow to generate the Yukawa coupling, (ii) induce a pNGB effective potential that realizes EWSB satisfactorily, (iii) preserve the parity P_η that guarantees the stability of our DM candidate η.

In addition to these necessary requirements, the choice of the SO(6) representation for Ψ also determines whether λ_ψ breaks or preserves the η shift symmetry $U(1)_\eta$, that is to say, whether or not ψ-loops contribute to the effective potential for η. This is crucial to determine the DM mass. To study this issue, it is useful to decompose the SO(6) multiplets under the maximal subgroup $SO(4) \times SO(2)_\eta \simeq SU(2)_L \times SU(2)_R \times U(1)_\eta$, where $SO(2)_\eta \simeq U(1)_\eta$ is precisely the symmetry associated with the NGB η, that is generated by $T_\eta = T^{\hat{5}}$ defined in eq. (A.2):

$$T_\eta = \frac{1}{\sqrt{2}} \begin{pmatrix} 0_{4\times4} & 0_{4\times2} \\ 0_{2\times4} & \sigma_2 \end{pmatrix} . \tag{A.12}$$

From eq. (A.6) and eq. (A.12) we have

$$[P_\eta, T_\eta] \neq 0 , \tag{A.13}$$

$\psi \setminus \Psi$	$\mathbf{1}$	$\mathbf{4}+\overline{\mathbf{4}}$	$\mathbf{6}$	$\mathbf{10}+\overline{\mathbf{10}}$	$\mathbf{15}$	$\mathbf{20'}$	$\dots$
q_L, l_L	$-$	$\times$	$\checkmark$	$\checkmark$	$\times$	$\times$	$\dots$
u_R, d_R, e_R	$\checkmark$	$\times$	$\times$	$\times$	$\checkmark$	$\checkmark$	$\dots$

Table 1. SO(6) representations for the spurions Ψ that can embed the SM fermions ψ preserving P_η. The symbol $\checkmark$ ($\times$) indicates that the P_η-preserving embedding does not break (does break) the $SO(2)_\eta$ subgroup.

therefore one cannot assign to the SM fields a definite P_η parity and a non-zero $U(1)_\eta$ charge at the same time. This means that both symmetries can be preserved by the SM couplings to the strong sector only if the SM fields transform trivially under the $SO(2)_\eta$, i.e. they are not charged under $U(1)_\eta$.
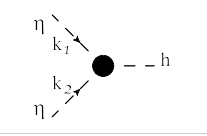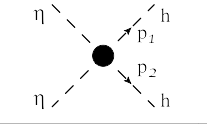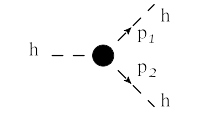
Let us classify the spurions Ψ that can accommodate the SM fermions while preserving P_η. The SM fermion isosinglets (isodoublets) can be embedded in any SO(6) representation that contains a singlet (doublet) of $SU(2)_L$. We find that an embedding preserving P_η is possible using a vector representation, $\Psi \sim \mathbf{1}$, $\mathbf{6}$, $\mathbf{15}$, $\mathbf{20'}$, ..., or a pair of spinor representations, $\mathbf{4}+\overline{\mathbf{4}}$, $\mathbf{10}+\overline{\mathbf{10}}$, and so on (when acting on spinors, P_η interchanges conjugate representations). Their $SU(2)_L \times SU(2)_R \times U(1)_\eta$ decomposition reads

$$
\begin{aligned}
\mathbf{4} &= (\mathbf{2},\mathbf{1})_{+1} \oplus (\mathbf{1},\mathbf{2})_{-1}\,, \\
\mathbf{6} &= (\mathbf{2},\mathbf{2})_0 \oplus (\mathbf{1},\mathbf{1})_{+2} \oplus (\mathbf{1},\mathbf{1})_{-2}\,, \\
\mathbf{10} &= (\mathbf{2},\mathbf{2})_0 \oplus (\mathbf{3},\mathbf{1})_{+2} \oplus (\mathbf{1},\mathbf{3})_{-2}\,, \\
\mathbf{15} &= (\mathbf{1},\mathbf{3})_0 \oplus (\mathbf{3},\mathbf{1})_0 \oplus (\mathbf{1},\mathbf{1})_0 \oplus (\mathbf{2},\mathbf{2})_{+2} \oplus (\mathbf{2},\mathbf{2})_{-2}\,, \\
\mathbf{20'} &= (\mathbf{3},\mathbf{3})_0 \oplus (\mathbf{2},\mathbf{2})_{+2} \oplus (\mathbf{2},\mathbf{2})_{-2} \oplus (\mathbf{1},\mathbf{1})_{+4} \oplus (\mathbf{1},\mathbf{1})_{-4} \oplus (\mathbf{1},\mathbf{1})_0\,. \quad \text{(A.14)}
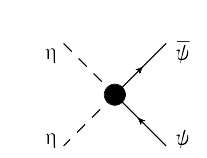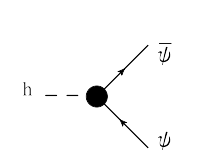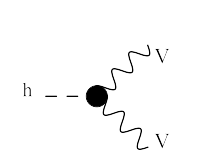\end{aligned}
$$

The components that can contain the SM fermions and do not transform under $U(1)_\eta$ are, for the isodoublets, the $(\mathbf{2},\mathbf{2})_0$ in the $\mathbf{6}$ or in the $\mathbf{10}$, and for the isosinglets either the $(\mathbf{1},\mathbf{1})_0$ or the $(\mathbf{1},\mathbf{3})_0$, which are present in the $\mathbf{1}$, the $\mathbf{15}$ or the $\mathbf{20'}$. These results are summarized in table 1.

In the following we will describe the properties of two models. In the first one we will embed all the SM fields in the $\mathbf{6}$ of SO(6), and therefore the right-handed couplings to the strong sector will break the $U(1)_\eta$ symmetry explicitly. The top quark loops will give the largest contributions to all terms of the pNGB effective potential in eq. (A.8); this corresponds to Case 1 of section 2. In the second model, on the other hand, we will embed the up-type quark singlets, and in particular t_R, in the $\mathbf{15}$, so that $U(1)_\eta$ will be preserved by the top couplings; doublets and down-type quark singlets will be embedded in the $\mathbf{6}$ as before. In this case the DM particle can be lighter than the EW scale leading to a substantially different phenomenology; this corresponds to Case 2. Both models satisfy the properties (i)-(iii) given above.

Before going to these two specific models, let us briefly mention an alternative way to keep η light. If the SM embedding in SO(6) representations preserves the SO(5) subgroup, that is broken by the Higgs VEV down to an $SO(4)'$, we would have after EWSB four exact

pNGB Interactions	Composite	Non-Composite
η, k_1, k_2, η — h	$-2iv\,\lambda\sqrt{1-\xi} + \dfrac{iv(k_1+k_2)^2}{f^2\sqrt{1-\xi}}$	$-2iv\,\lambda$
η, h, p_1, p_2, η, h	$-2i\,\lambda(1-\xi) + \dfrac{i(1+\xi)(p_1+p_2)^2}{f^2(1-\xi)} - \dfrac{2i\,\xi\;p_1\cdot p_2}{f^2(1-\xi)}$	$-2i\,\lambda$
h — h, p_1, p_2, h	$-\dfrac{3im_h^2}{v}\sqrt{1-\xi} + \dfrac{2iv}{f^2\sqrt{1-\xi}}\,[(p_1+p_2)^2 - p_1\cdot p_2]$	$-\dfrac{3im_h^2}{v}$

pNGB/SM Int.	Composite		Non-Composite
η, $\bar{\psi}$, η, ψ	$\dfrac{\sqrt{2}\,iv y_\psi}{f^2}\big[\mathrm{Re}(c_\psi) + i\,\mathrm{Im}(c_\psi)\gamma^5\big]$	$\psi_R \in \mathbf{6}$	0
	0	$\psi_R \in \mathbf{15}$	
h, $\bar{\psi}$, ψ	$\dfrac{-iy_\psi}{\sqrt{2}}\,\dfrac{1-2\xi}{\sqrt{1-\xi}}$	$\psi_R \in \mathbf{6}$	$\dfrac{-iy_\psi}{\sqrt{2}}$
	$\dfrac{-iy_\psi}{\sqrt{2}}\,\sqrt{1-\xi}$	$\psi_R \in \mathbf{15}$	
h, V, V	$igm_W\sqrt{1-\xi}$	$V = W$	igm_W $\quad V = W$
	$\dfrac{igm_Z}{c_W}\sqrt{1-\xi}$	$V = Z$	$\dfrac{igm_Z}{c_W}$ $\quad V = Z$

Table 2. Feynman rules for the relevant interactions between the Higgs boson h and the DM particle η (upper panel) and for the interactions of h and η with the SM fermions and gauge bosons (lower panel). The second column corresponds to the composite model with coset $O(6)/O(5)$, while the third column corresponds to the SM plus a real scalar singlet.

NGBs, the three SM ones eaten by the weak gauge bosons plus η. In this case the mass of η would be protected by this $SO(4)'$ symmetry and not by the $SO(2)_\eta$ of eq. (A.12). It is clear, however, that the SM fermion doublets cannot be embedded in complete $SO(5)$ representations, so η gets always a mass from loops of this sector. A relative light η could be achieved by requiring the smallest possible coupling of the fermion doublets to the strong sector. Here we do not explore this possibility any further.

A.1 Case 1: all the SM fermions in the representation 6

Let us begin with embedding all SM fermions into $\Psi \sim \mathbf{6}$ [10]. A SM electroweak doublet can be embedded in the the bi-doublet with $P_\eta = +1$, while for a SM isosinglet the only embedding with $P_\eta = +1$ (to avoid the breaking of P_η) is given by $\Psi_{\psi_R} = (0,0,0,0,0,\psi_R)$. Coming to the $U(1)_X$ assignments, recall that the pNGB field Σ does not carry X-charge. Using eq. (A.10), the isosinglet up-type and down-type quarks should respectively be embedded into a spurion with $X_{u_R} = 2/3$ and $X_{d_R} = -1/3$. Then, in order to allow for the Yukawa couplings to Σ, the isodoublet quarks q_L should be embedded into two spurions, one with $X_{q_L} = 2/3$ to generate the up-quark Yukawa, $y_u \simeq \lambda_{q_L}\lambda_{u_R}/g_\rho$, and one with $X_{q'_L} = -1/3$ to generate the down-quark Yukawa, $y_d \simeq \lambda_{q'_L}\lambda_{d_R}/g_\rho$.[5] Here and in the following we tacitly assume that the lepton couplings to the composite sector are generated in analogy with the quark ones.

As can be seen from the $U(1)_\eta$ charges of the $\mathbf{6}$ components in eq. (A.14), the η shift symmetry is broken by the embedding of the right-handed quarks. Therefore η will receive an effective potential from loops involving only isosinglet quarks. This can be seen explicitly by writing all the invariants that involve the quarks and the pNGBs. The techniques of refs. [55, 56] are useful to count the number of possible invariants, that we write using the spurion notation

$$(\bar{\Psi}_{q_L}\Sigma)(\Sigma^T\Psi_{u_R}) = \frac{1}{\sqrt{2}}\bar{u}_L u_R\, h\sqrt{1-\eta^2-h^2}\,,$$

$$(\bar{\Psi}_{q'_L}\Sigma)(\Sigma^T\Psi_{d_R}) = -\frac{1}{\sqrt{2}}\bar{d}_L d_R\, h\sqrt{1-\eta^2-h^2}\,,$$

$$(\bar{\Psi}_{u_R}\Sigma)\,\slashed{p}(\Sigma^T\Psi_{u_R}) = \bar{u}_R\,\slashed{p}u_R(1-\eta^2-h^2)\,,$$

$$(\bar{\Psi}_{d_R}\Sigma)\,\slashed{p}(\Sigma^T\Psi_{d_R}) = \bar{d}_R\,\slashed{p}d_R(1-\eta^2-h^2)\,,$$

$$(\bar{\Psi}_{q_L}\Sigma)\,\slashed{p}(\Sigma^T\Psi_{q_L}) = \frac{1}{2}\bar{u}_L\,\slashed{p}u_L\, h^2\,,$$

$$(\bar{\Psi}_{q'_L}\Sigma)\,\slashed{p}(\Sigma^T\Psi_{q'_L}) = \frac{1}{2}\bar{d}_L\,\slashed{p}d_L\, h^2\,. \tag{A.15}$$

We can now justify the parameterization of eq. (2.9) for the DM−bottom coupling. The first and second lines in eq. (A.15) generate the quark masses and, at order η^2, they also give a contribution to the couplings of eq. (2.3), $\Delta c_u = \Delta c_d = 1/2$, up to $\mathcal{O}(\xi)$ corrections. The third and fourth lines in eq. (A.15) correspond to derivative couplings analog to the one in eq. (2.5), that can be cast in the form of eq. (2.3) by using the Dirac equation. Using NDA to estimate the coefficients of these invariants, one obtains $\Delta c_{u,d} = O(\lambda^2_{u_R,d_R}/g_\rho^2) + i\,O(\lambda^2_{u_R,d_R}/g_\rho^2)$. Note that the ratio $\lambda^2_{u_R,d_R}/g_\rho^2$ varies approximately in the range $[y^2_{u,d}/g_\rho^2, 1]$, depending on the relative size of λ_{q_L,q'_L} and λ_{u_R,d_R}. Adding the two contributions to the DM−fermion couplings, one recovers eq. (2.9).[6]

---

[5]In the case of the third family, the coupling $\lambda_{q'_L}$ implies a correction to the SM value of the coupling $Zb_L\overline{b_L}$, because it corresponds to $T^3_R(b_L) = 1/2$ different from $T^3_L(b_L) = -1/2$ [57]; we assume a small value $\lambda_{q'_L} \sim y_b$, to guarantee a small enough correction to $Zb_L\overline{b_L}$.

[6]In general, the contributions of order $\lambda^2_{u_R,d_R}/g_\rho^2$ could have negative sign and partially compensate the contribution $1/2$. In our analysis we did not consider the possibility of such a cancellation.

The Feynman rules for the interactions of η and h with fermions, following from eq. (A.15), are reported in table 2.

The effective lagrangian in momentum space, obtained after integrating out the composite sector, can be written as

$$\mathcal{L}_{\rm f} = \sum_{r=q_L,u_R,q'_L,d_R} \left[\Pi_0^r(p^2)(\bar{\Psi}_r \,\slashed{p}\, \Psi_r) - \Pi_1^r(p^2)(\bar{\Psi}_r \Sigma) \,\slashed{p}\, (\Sigma^T \Psi_r) \right]$$
$$- \left[M^u(p^2)(\bar{\Psi}_{q_L} \Sigma)(\Sigma^T \Psi_{u_R}) + M^d(p^2)(\bar{\Psi}_{q'_L} \Sigma)(\Sigma^T \Psi_{d_R}) + h.c. \right] , \qquad \text{(A.16)}$$

where p is the momentum of the fermion fields. Parametrically, at small momentum ($p \lesssim m_\rho$) we have

$$\Pi_0^r \simeq 1, \qquad \Pi_1^r \simeq \frac{\lambda_r^2}{g_\rho^2}, \qquad M^u \simeq \frac{\lambda_{q_L} \lambda_{u_R}}{g_\rho} f, \qquad M^d \simeq \frac{\lambda_{q'_L} \lambda_{d_R}}{g_\rho} f . \qquad \text{(A.17)}$$

Eqs. (A.15) and (A.16) imply that the fermion masses read $m_{u,d} = M^{u,d}(0)/\sqrt{2}(v/f)\sqrt{1-\xi}$. Loops of SM fermions contribute to the Coleman-Weinberg potential for the pNGBs. Since the heaviest fermions give the dominant contribution, we concentrate on the third family of quarks. At one-loop, from eq. (A.16) one obtains

$$V_{t,b}^{(6)}(h,\eta) = -2N_c \int \frac{d^4p}{(2\pi)^4} \left\{ \log\left[p^2 \left(\Pi_0^{q_L} + \Pi_0^{q'_L} - \frac{\Pi_1^{q_L}}{2} h^2 \right) \left(\Pi_0^{t_R} - \Pi_1^{t_R}(1 - \eta^2 - h^2) \right) \right. \right.$$
$$\left. \left. - \frac{|M^t|^2}{2} h^2 (1 - \eta^2 - h^2) \right] + \log[(q_L, t_R) \leftrightarrow (q'_L, b_R)] \right\} , \quad \text{(A.18)}$$

where the overall negative sign comes from the fermion loop, the factor of 2 from the fermion polarizations and N_c is the number of colors.

For a momentum larger than the mass of the resonances m_ρ, one expects the form factors Π_1^r and M^t to fall off fast enough to make the integral in eq. (A.18) convergent. At $p \lesssim m_\rho$, for $\lambda_r \ll g_\rho$ one can expand the logarithm in eq. (A.18), since each power of h^2 and η^2 is associated with a suppression factor $(\lambda_r \lambda_{r'}/g_\rho^2)$. One can easily check that all terms in the expansions in h^2 and η^2 receive contributions from the top couplings λ_{q_L} and λ_{t_R}, therefore one can safely neglect the terms in $\lambda_{q'_L}$ and λ_{b_R}, that we assume to be of the order of the bottom Yukawa. The first logarithm in eq. (A.18) provides the dominant contribution, coming from the top-quark, to the effective potential $V_{\rm eff}$ defined in eq. (A.8). By expanding this contribution and integrating over momenta, we obtain

$$\mu_h^2 = \frac{N_c m_\rho^2}{16\pi^2} \left(c_1 \lambda_{q_L}^2 - 2c_2 \lambda_{t_R}^2 - 2c_3 y_t^2 \right) ,$$
$$\lambda_h = \frac{N_c}{16\pi^2} \left(4c_3 y_t^2 g_\rho^2 + \frac{1}{2} c_1^{(2)} \lambda_{q_L}^4 + 2c_2^{(2)} \lambda_{t_R}^4 \right) ,$$
$$\mu_\eta^2 = \frac{N_c m_\rho^2}{16\pi^2} \left(-2c_2 \lambda_{t_R}^2 \right) ,$$
$$\lambda_\eta = \frac{N_c}{16\pi^2} \left(2c_2^{(2)} \lambda_{t_R}^4 \right) ,$$
$$\lambda = \frac{N_c}{16\pi^2} \left(2c_3 y_t^2 g_\rho^2 + 2c_2^{(2)} \lambda_{t_R}^4 \right) , \qquad \text{(A.19)}$$

where c_i and $c_i^{(2)}$ are order one coefficients that account for the uncertainty in the integrals over the form factors. More specifically, the $c_i^{(2)}$ come from the second order in the log expansion, and therefore they involve an integral over a higher power of the form factors, that in some explicit models is suppressed (see e.g. ref. [58]); in the following we neglect for simplicity these terms, when compared to the c_i ones.

In order for $\xi = -\mu_h^2/(\lambda_h f^2)$ to be smaller than one, a partial cancellation is needed between the terms in μ_h^2, that requires $\lambda_{t_R} \sim \lambda_{q_L}$.[7] Then, from eq. (A.19), using $y_t \simeq \lambda_{q_L} \lambda_{t_R}/g_\rho$ and eq. (A.9), the Higgs mass can be written as

$$ m_h^2 = c_3 \frac{N_c}{2\pi^2} \, y_t^2 \, \xi \, m_\rho^2 \simeq c_3 (250 \text{ GeV})^2 \, \frac{\xi}{0.1} \left(\frac{m_\rho}{2 \text{ TeV}} \right)^2 \, . \tag{A.20} $$

The coupling λ is generated by the same term that controls also λ_h, so we expect it to be positive and of the same order

$$ \lambda \simeq \frac{\lambda_h}{2} = \frac{m_h^2}{4v^2} \tag{A.21} $$

(for $m_h = 125 \text{ GeV}$ this corresponds to $\lambda \simeq 1/16$). The singlet mass can be written as

$$ m_\eta^2 \simeq \mu_\eta^2 = c_2 \frac{N_c}{8\pi^2} \, \lambda_{t_R}^2 \, m_\rho^2 \simeq m_h^2 \frac{c_2}{c_3} \frac{\lambda_{t_R}^2}{4 y_t^2 \xi} \, . \tag{A.22} $$

Since the last factor in eq. (A.22) is larger than one, η is generically heavier than the Higgs.

A.2 Case 2: the right-handed top quark in the representation 15

As mentioned above, if t_R is embedded into an SO(6) representation preserving $\mathrm{U}(1)_\eta$, the DM η is naturally lighter than the Higgs. In this section we provide an example of such a model, where up-type isosinglet quarks are embedded in the **15**.[8] As in the previous section we keep all isodoublets and down-type isosinglets in the **6**. The up-type Yukawa can be generated when u_R is embedded in the $(\mathbf{1},\mathbf{3})_\mathbf{0} \subset \mathbf{15}$. Taking for definiteness $X_{q_L} = 2/3$, in the up-type quark sector eq. (A.15) is replaced by

$$ \bar{\Psi}_{q_L} \Psi_{u_R} \Sigma = \frac{1}{2\sqrt{2}} \bar{u}_L u_R \, h \, , $$

$$ \Sigma^T \bar{\Psi}_{u_R} \, p\!\!\!/ \, \Psi_{u_R} \Sigma = \frac{1}{4} \bar{u}_R \, p\!\!\!/ \, u_R \, h^2 \, , $$

$$ (\bar{\Psi}_{q_L} \Sigma) \, p\!\!\!/ \, (\Sigma^T \Psi_{q_L}) = \frac{1}{2} \bar{u}_L \, p\!\!\!/ \, u_L \, h^2 \, . \tag{A.23} $$

As expected, no terms involving η are generated, therefore the DM−top coupling c_t of eq. (2.3) vanishes, and there are no loop contributions to the effective potential for η from the up-quark sector.

---

[7]We are neglecting gauge contributions that are smaller than the top one.

[8]Embedding t_R in the **1** of SO(6) is the simplest possibility for light DM, but it is not satisfactory for EWSB, because in this case t_R does not break the Higgs shift symmetry either. As a consequence, one needs to invoke a cancellation in the strong sector to obtain $v \ll f$, and moreover the Higgs mass tends to be too small.

There are still, however, DM couplings to the down-type quarks; the heaviest is the bottom, therefore eq. (A.22) is replaced by

$$m_\eta^2 \simeq \mu_\eta^2 = c_2' \frac{N_c}{8\pi^2} \lambda_{b_R}^2 m_\rho^2 , \qquad (A.24)$$

which results in a DM mass $m_\eta \gtrsim O(10)\,\text{GeV}$ ($\lambda_{b_R} \gtrsim y_b \simeq 1/40$). Notice that, by embedding also the b_R in the **15**, we could make the DM even lighter. Note also that the DM$-$Higgs coupling λ is correlated to the DM mass,

$$\frac{m_\eta^2}{\lambda f^2} \simeq \frac{g_\rho^2}{\max(\lambda_{b_L}^2, \lambda_{b_R}^2)} \gg 1 , \qquad (A.25)$$

in agreement with the general expectation of eq. (2.6). Therefore, the lightest the DM is, the weakest its Higgs portal interaction becomes.

Similarly to the previous model, starting from eq. (A.23) one can compute the top quark contribution to the effective potential,

$$V_t^{(\mathbf{15})}(h) = -2N_c \int \frac{d^4p}{(2\pi)^4} \log \left[p^2 \left(\Pi_0^q - \frac{\Pi_1^q}{2} h^2 \right) \left(\Pi_0^t - \frac{\Pi_1^t}{4} h^2 \right) - \frac{|M^t|^2}{8} h^2 \right] . \qquad (A.26)$$

Expanding and integrating the logarithm, one finds

$$\mu_h^2 = \frac{N_c m_\rho^2}{16\pi^2} \left(c_1 \lambda_{q_L}^2 + \frac{1}{2} c_2 \lambda_{t_R}^2 - 2c_3 y_t^2 \right) ,$$

$$\lambda_h = \frac{N_c}{16\pi^2} \left(\frac{1}{2} c_1^{(2)} \lambda_{q_L}^4 + \frac{1}{8} c_2^{(2)} \lambda_{t_R}^4 + c_3^{(2)} y_t^4 \log \frac{m_\rho^2}{m_t^2} - 2c_4 \lambda_{q_L}^2 y_t^2 - c_5 \lambda_{t_R}^2 y_t^2 \right) , \qquad (A.27)$$

where c_i are coefficients of order one. As in the previous model, in order to obtain $v \ll f$ we need a partial cancellation between the different terms of μ_h^2, that can be achieved if $\lambda_{q_L} \sim \lambda_{t_R} \sim \sqrt{y_t g_\rho}$ (and if c_1 and c_2 have opposite sign). In this case the dominant terms in the quartic Higgs couplings are expected to be those proportional to $c_{1,2}^{(2)} \sim 1$, that lead to a Higgs mass

$$m_h^2 \sim \frac{N_c}{4\pi^2} y_t^2 \xi m_\rho^2 = (170\,\text{GeV})^2 \frac{\xi}{0.1} \left(\frac{m_\rho}{2\,\text{TeV}} \right)^2 . \qquad (A.28)$$

In summary, EWSB can be smoothly obtained when t_R is embedded in the **15**, with a Higgs naturally close to the presently favoured low-mass region.

B Dark matter annihilation cross sections

In this appendix we outline the calculation of the relic density and collect for completeness all relevant cross sections. Following the standard recipe [16], the central ingredient in the calculation of the DM relic density is the thermal-average of its total annihilation cross section times the relative velocity v_{rel},

$$\langle \sigma v_{\text{rel}} \rangle = \frac{m_\eta}{64\pi^4 x\, n_{\text{EQ}}^2} \int_{4m_\eta^2}^\infty ds\, \hat{\sigma}(s) \sqrt{s - 4m_\eta^2}\, \mathcal{K}_1 \left(x\sqrt{s}/m_\eta \right) , \qquad (B.1)$$

where $\hat{\sigma}(s) \equiv sv_{\rm rel} \sum_F \sigma(\eta\eta \to F)$, being $\sigma(\eta\eta \to F)$ the annihilation cross section into the SM final state F. In eq. (B.1) the equilibrium number density for η is given by

$$n_{\rm EQ} = \frac{m_\eta^3 \mathcal{K}_2(x)}{2\pi^2 x} \ . \tag{B.2}$$

Here $\mathcal{K}_{1,2}$ are the modified Bessel function and $x \equiv m_\eta/T$, where T is the temperature. A Boltzmann equation describes the evolution of the number density $n(x)$ of the DM particle during the expansion of the Universe,

$$\frac{d{\rm Y}}{dx} = -\frac{xs(x)}{H}\langle \sigma v_{\rm rel}\rangle \left({\rm Y}^2 - {\rm Y}_{\rm EQ}^2\right) \ , \tag{B.3}$$

where the yield is defined by ${\rm Y} \equiv n(x)/s(x)$, and the entropy density $s(x)$ is given by

$$s(x) = \frac{2\pi^2 g_* m_\eta^3}{45 x^3} \ . \tag{B.4}$$

The Hubble parameter evaluated at $x = 1$ is given by

$$H = \sqrt{\frac{4\pi^3 g_*}{45}} \frac{m_\eta^2}{M_{\rm PL}} \ , \tag{B.5}$$

the value of the Planck mass is $M_{\rm PL} = 1.22 \cdot 10^{19}\,{\rm GeV}$, and g_* is the effective number of degrees of freedom. The integration of eq. (B.3), from $x = 0$ to the present value $x_0 = m_\eta/T_0$, gives the DM yield today, ${\rm Y}_0$, which in turns is related to the DM relic density [17],

$$\Omega_\eta h^2 = \frac{2.74 \cdot 10^8 m_\eta {\rm Y}_0}{\rm GeV} = 0.1126 \pm 0.0036 \ . \tag{B.6}$$

The computation of the annihilation cross sections makes use of the Feynman rules collected in table 2. The relevant final states are the heavy fermions (the t, b, c quarks, as well as the τ lepton), the electroweak gauge bosons and the Higgs. Defining $\hat{\sigma}_{\eta\eta}(F) \equiv sv_{\rm rel}\sigma(\eta\eta \to F)$, we find

$$\hat{\sigma}_{\eta\eta}(\psi\bar{\psi})|_{\psi_R \in \mathbf{6}} = \frac{N_c\, m_\psi^2 \sqrt{1 - 4m_\psi^2/s}}{\pi f^4}\left\{s{\rm Im}(c_\psi)^2 + (s - 4m_\psi^2)\right. \tag{B.7}$$

$$\left. \times \left[{\rm Re}(c_\psi)^2 + \frac{\Gamma(1-2\xi)^2}{4(1-\xi)^2} + {\rm Re}(c_\psi)\frac{(s-m_h^2)\left[s - 2\lambda f^2(1-\xi)\right](1-2\xi)}{\left[(s-m_h^2)^2 + \Gamma_h^2 m_h^2\right](1-\xi)}\right]\right\},$$

$$\hat{\sigma}_{\eta\eta}(\psi\bar{\psi})|_{\psi_R \in \mathbf{15}} = \frac{N_c m_\psi^2 (s - 4m_\psi^2)^{3/2}\Gamma}{4\pi f^4 \sqrt{s}} \ , \tag{B.8}$$

$$\hat{\sigma}_{\eta\eta}(WW) = \frac{s^2\,\Gamma}{8\pi f^4}\left(1 - \frac{4m_W^2}{s} + \frac{12m_W^4}{s^2}\right)\sqrt{1 - \frac{4m_W^2}{s}} \ , \tag{B.9}$$

$$\hat{\sigma}_{\eta\eta}(ZZ) = \frac{s^2\,\Gamma}{16\pi f^4}\left(1 - \frac{4m_Z^2}{s} + \frac{12m_Z^4}{s^2}\right)\sqrt{1 - \frac{4m_Z^2}{s}} \ , \tag{B.10}$$

$$\hat{\sigma}_{\eta\eta}(hh) = \frac{\sqrt{1 - 4m_h^2/s}}{16f^8\pi(1-\xi^2)^2(s-m_h^2)\left[m_h^4 + m_\eta^2(s-4m_h^2)\right]} \tag{B.11}$$

$$\times \left\{ \frac{8f^2\xi\left[m_h^4 + m_\eta^2(s-4m_h^2)\right]\operatorname{arctanh}(\Delta)\left[m_h^2 - 2\lambda f^2(1-\xi)\right]^2}{(s-2m_h^2)^2\Delta} A_{\eta\eta} + B_{\eta\eta} \right\},$$

where we defined the ratios

$$\Delta \equiv \frac{\sqrt{s-4m_\eta^2}\sqrt{s-4m_h^2}}{s-2m_h^2}, \quad \Gamma \equiv \frac{\left[s-2\lambda f^2(1-\xi)\right]^2}{(s-m_h^2)^2 + \Gamma_h^2 m_h^2}. \tag{B.12}$$

The lengthy expressions for the functions $A_{\eta\eta}$ and $B_{\eta\eta}$ are listed at the end of this appendix.

Notice that taking the limit $f \to \infty$, we recover the known expressions for the annihilation cross sections in the non-composite case,

$$\hat{\sigma}_{\eta\eta}(\psi\overline{\psi})\big|_{f\to\infty} = \frac{N_c\,\lambda^2 m_\psi^2 (s-4m_\psi^2)^{3/2}}{\pi\sqrt{s}[(s-m_h^2)^2 + \Gamma_h^2 m_h^2]}, \tag{B.13}$$

$$\hat{\sigma}_{\eta\eta}(WW)\big|_{f\to\infty} = \frac{s^2\lambda^2}{2\pi\left[(s-m_h^2)^2 + \Gamma_h^2 m_h^2\right]}\left(1 - \frac{4m_W^2}{s} + \frac{12m_W^4}{s^2}\right)\sqrt{1 - \frac{4m_W^2}{s}}, \tag{B.14}$$

$$\hat{\sigma}_{\eta\eta}(ZZ)\big|_{f\to\infty} = \frac{s^2\lambda^2}{4\pi\left[(s-m_h^2)^2 + \Gamma_h^2 m_h^2\right]}\left(1 - \frac{4m_Z^2}{s} + \frac{12m_Z^4}{s^2}\right)\sqrt{1 - \frac{4m_Z^2}{s}}, \tag{B.15}$$

$$\hat{\sigma}_{\eta\eta}(hh)\big|_{f\to\infty} = \frac{\lambda^2\sqrt{1 - 4m_h^2/s}}{4\pi}\left(\mathcal{A}_{\eta\eta} + \mathcal{B}_{\eta\eta}\,v^2 + \mathcal{C}_{\eta\eta}\,v^4\right), \tag{B.16}$$

where

$$\mathcal{A}_{\eta\eta} = \frac{(s+2m_h^2)^2}{(s-m_h^2)^2}, \tag{B.17}$$

$$\mathcal{B}_{\eta\eta} = -\frac{16\lambda(s+2m_h^2)\operatorname{arctanh}(\Delta)}{\Delta(s-2m_h^2)(s-m_h^2)}, \tag{B.18}$$

$$\mathcal{C}_{\eta\eta} = 32\lambda^2\left[\frac{\operatorname{arctanh}(\Delta)}{\Delta(s-2m_h^2)^2} + \frac{1}{4m_\eta^2(s-4m_h^2) + 4m_h^4}\right]. \tag{B.19}$$

We plot the annihilation cross sections in figure 8, as a function of the DM mass, for $v_{\rm rel} = 2/3$, $\lambda = 10^{-2}$ and $m_h = 125\,{\rm GeV}$, taking $f = 500\,{\rm GeV}$ in the left-hand panel and $f = \infty$ in the right-hand panel. For comparison we also show (black dashed line) the typical value for $\langle\sigma v_{\rm rel}\rangle$ suggested by eq. (3.1), needed for the thermal freeze-out of the DM particle. In the left panel of figure 8 one can distinguish the four DM mass regions described in section 3, that characterize the qualitative behavior of the composite singlet relic density.

Finally we report the expressions for the coefficients $A_{\eta\eta}$ and $B_{\eta\eta}$ in eq. (B.11):

$$A_{\eta\eta} = f^2\left\{m_h^4\left[4f^2\lambda(\xi-1)(3\xi-2) + (5\xi-4)s\right] - m_h^2\xi\left[s + 2f^2\lambda(1-\xi)\right]^2\right.$$
$$\left. + (1-\xi)s\left[4f^4\lambda^2(1-\xi)\xi - 2f^2\lambda(1-2\xi)s + s^2\right] + 3m_h^6\xi\right\}, \tag{B.20}$$

$$B_{\eta\eta} = \frac{f^4}{s-m_h^2}\sum_{n=0}^{6} g_{2n}\,m_h^{2n}, \tag{B.21}$$
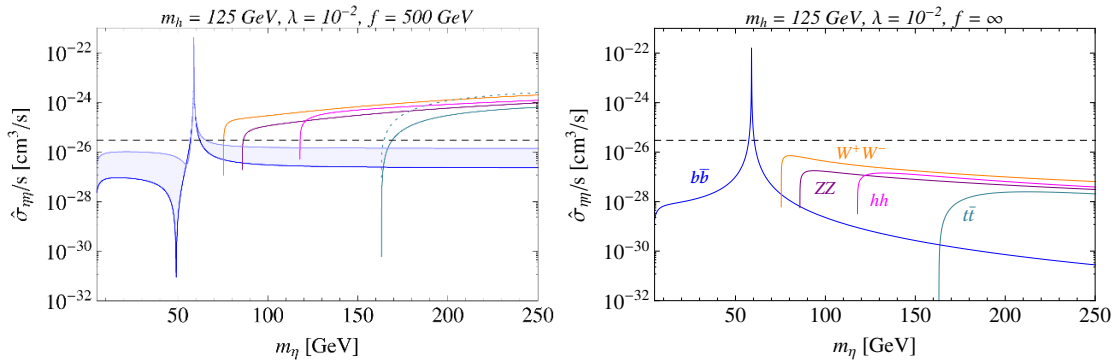
Figure 8. Annihilation cross sections times the relative velocity v_{rel} for the DM candidate η. We plot eqs. (B.7)–(B.11) for $f = 500\,\text{GeV}$ (left-hand panel), and eqs. (B.13)–(B.16) for the non-composite case (right-hand panel); in both cases $\lambda = 10^{-2}$, $m_h = 125\,\text{GeV}$, $v_{\text{rel}} = 2/3$. We vary the coefficient c_b as in figure 1. For the top quark channel, we show both Case 1 and 2 (dotted and solid cyan lines, respectively). The black dashed line indicates the benchmark value for DM freeze-out, $\langle \sigma v_{\text{rel}} \rangle = 3 \cdot 10^{-26}\ \text{cm}^3\text{s}^{-1}$.

with

$$g_0 = (1 - \xi)^2 s^2 \left\{ 32 f^8 \lambda^4 (1 - \xi)^2 \xi^2 + m_\eta^2 s \left[2 f^2 \lambda (2\xi - 1) + s \right]^2 \right\} , \tag{B.22}$$

$$g_2 = 2 s (\xi - 1) \xi \left\{ m_\eta^2 s^2 \left[2 f^2 \lambda (2\xi - 1) + s \right] + 32 f^6 \lambda^3 (\xi - 1)^2 \xi \left[s - f^2 \lambda (\xi - 1) \right] \right\} , \tag{B.23}$$

$$g_4 = (\xi - 1)^2 \left\{ 32 f^8 \lambda^4 (\xi - 1)^2 \xi^2 - 128 f^6 \lambda^3 (\xi - 1) \xi^2 s + 4 f^4 \lambda^2 [4\xi(4\xi - 1) + 1] s^2 + \right.$$
$$\left. 4 f^2 \lambda (2\xi - 1) s^3 + s^4 \right\} - m_\eta^2 s \left\{ 48 f^4 \lambda^2 \left(2\xi^2 - 3\xi + 1 \right)^2 + \right.$$
$$\left. 48 f^2 \lambda (\xi - 1)^2 (2\xi - 1) s + [\xi(11\xi - 24) + 12] s^2 \right\} , \tag{B.24}$$

$$g_6 = 2(\xi - 1) \left\{ 32 f^6 \lambda^3 (\xi - 1)^2 \xi^2 - 8 f^4 \lambda^2 (\xi - 1) [2\xi(\xi + 2) - 1] s - \right.$$
$$4 m_\eta^2 \left[2 f^2 \lambda (2\xi - 1) + s \right] \left[4 f^2 \lambda (\xi - 1)(2\xi - 1) + (5\xi - 2) s \right] +$$
$$\left. 2 f^2 \lambda [\xi(14\xi - 13) + 4] s^2 + (3\xi - 2) s^3 \right\} , \tag{B.25}$$

$$g_8 = 16 f^2 \lambda (\xi - 1) \left\{ f^2 \lambda (\xi - 1) [\xi(7\xi - 4) + 1] + 4 m_\eta^2 (1 - 2\xi) \xi \right\} +$$
$$4 s \left\{ 4 f^2 \lambda (\xi - 1) [2(\xi - 2)\xi + 1] + m_\eta^2 (8 - 11\xi) \xi \right\} + (3\xi - 2)(5\xi - 2) s^2 , \tag{B.26}$$

$$g_{10} = 8\xi \left[2 f^2 \lambda (\xi - 1)(3\xi - 1) - 2 m_\eta^2 \xi + (\xi - 1) s \right] , \tag{B.27}$$

$$g_{12} = 6 \xi^2 . \tag{B.28}$$

C Dark matter scattering cross section on nuclei

The spin-independent elastic scattering cross section of a real scalar η on a nucleus can be parameterized as

$$\sigma_{\text{SI}} = \frac{1}{\pi} \left(\frac{m_\eta m_n}{m_\eta + m_n} \right)^2 \frac{[Z f_p + (A - Z) f_n]^2}{A^2} , \tag{C.1}$$

where m_n is the neutron mass, Z and $A - Z$ are the number of protons and neutrons in the nucleus, and the function f_p (f_n) describes the coupling between η and protons (neutrons):

$$f_{n,p} = \sum_{q=u,d,s} f_{T_q}^{(n,p)} a_q \frac{m_{n,p}}{m_q} + \frac{2}{27} f_{T_G}^{(n,p)} \sum_{q=c,b,t} a_q \frac{m_{n,p}}{m_q} . \tag{C.2}$$

The hadron matrix elements $f_{T_q}^{(n,p)}$ parametrize the quark content of the nucleon. They are extracted from pion-nucleon diffusion measurements. Following a recent analysis [59] we take

$$f_{T_u}^{(p)} = 0.017 , \qquad f_{T_d}^{(p)} = 0.022 , \qquad f_{T_s}^{(p)} = 0.053 , \tag{C.3}$$

$$f_{T_u}^{(n)} = 0.011 , \qquad f_{T_d}^{(n)} = 0.034 , \qquad f_{T_s}^{(n)} = 0.053 . \tag{C.4}$$

The DM couples also to the gluons in the nucleus, through a loop of heavy quarks (those with $m_q \gg \Lambda_{QCD}$). The corresponding matrix element is given by

$$f_{T_G}^{(n,p)} = 1 - \sum_{q=u,d,s} f_{T_q}^{(n,p)} . \tag{C.5}$$

In eq. (C.2), the parameter a_q describes the short-distance effective interactions between η and a given quark, normalized as

$$\mathcal{L}_\eta \supset \sum_q a_q \eta^2 \bar{q} q . \tag{C.6}$$

In our composite model there are two sources for this effective interaction: the direct coupling c_q of η to quarks, and a coupling mediated by the exchange of the Higgs boson. More precisely, only $\mathrm{Re}(c_q)$ enters in a_q, and thus contributes to σ_{SI}, while $\mathrm{Im}(c_q)$ leads to a coupling $\eta^2 \bar{q} \gamma_5 q$, that contributes only to the spin-dependent cross section. Coming to the Higgs in the t-channel, one should notice that the momentum transfer q^2 in the elastic scattering is very small, therefore the Higgs-exchange reduces to a contact interaction suppressed by m_h^2. In addition, the derivative coupling between η and h can be neglected, because it is proportional to q^2, and one is left with the coupling λ only. All in all, we find

$$a_q|_{q_R \in \mathbf{6}} = \frac{m_q}{m_\eta} \left[\frac{\mathrm{Re}(c_q)}{f^2} + \frac{\lambda(1 - 2\xi)}{m_h^2} \right] , \tag{C.7}$$

$$a_q|_{q_R \in \mathbf{15}} = \frac{m_q}{m_\eta} \frac{\lambda(1 - \xi)}{m_h^2} . \tag{C.8}$$

Putting all the ingredients together, one recovers the numerical approximation shown in eq. (5.1).

Open Access. This article is distributed under the terms of the Creative Commons Attribution License which permits any use, distribution and reproduction in any medium, provided the original author(s) and source are credited.

References

[1] V. Silveira and A. Zee, *Scalar phantoms*, *Phys. Lett.* **B 161** (1985) 136 [INSPIRE].

[2] J. McDonald, *Gauge singlet scalars as cold dark matter*, *Phys. Rev.* **D 50** (1994) 3637 [hep-ph/0702143] [INSPIRE].

[3] C. Burgess, M. Pospelov and T. ter Veldhuis, *The minimal model of nonbaryonic dark matter: a singlet scalar*, *Nucl. Phys.* **B 619** (2001) 709 [hep-ph/0011335] [INSPIRE].

[4] C.E. Yaguna, *Gamma rays from the annihilation of singlet scalar dark matter*, *JCAP* **03** (2009) 003 [arXiv:0810.4267] [INSPIRE].

[5] M. Farina, D. Pappadopulo and A. Strumia, *CDMS stands for constrained dark matter singlet*, *Phys. Lett.* **B 688** (2010) 329 [arXiv:0912.5038] [INSPIRE].

[6] W.-L. Guo and Y.-L. Wu, *The real singlet scalar dark matter model*, *JHEP* **10** (2010) 083 [arXiv:1006.2518] [INSPIRE].

[7] Y. Mambrini, *Higgs searches and singlet scalar dark matter: Combined constraints from XENON100 and the LHC*, Phys. Rev. **D 84** (2011) 115017 [arXiv:1108.0671] [INSPIRE].

[8] A. Djouadi, O. Lebedev, Y. Mambrini and J. Quevillon, *Implications of LHC searches for Higgs-portal dark matter*, Phys. Lett. **B 709** (2012) 65 [arXiv:1112.3299] [INSPIRE].

[9] K. Agashe, R. Contino and A. Pomarol, *The minimal composite Higgs model*, *Nucl. Phys.* **B 719** (2005) 165 [hep-ph/0412089] [INSPIRE].

[10] B. Gripaios, A. Pomarol, F. Riva and J. Serra, *Beyond the minimal composite Higgs model*, *JHEP* **04** (2009) 070 [arXiv:0902.1483] [INSPIRE].

[11] J. Galloway, J.A. Evans, M.A. Luty and R.A. Tacchi, *Minimal conformal technicolor and precision electroweak tests*, *JHEP* **10** (2010) 086 [arXiv:1001.1361] [INSPIRE].

[12] T.A. Ryttov and F. Sannino, *Ultra minimal technicolor and its dark matter TIMP*, *Phys. Rev.* **D 78** (2008) 115010 [arXiv:0809.0713] [INSPIRE].

[13] Y. Hosotani, P. Ko and M. Tanaka, *Stable Higgs bosons as cold dark matter*, *Phys. Lett.* **B 680** (2009) 179 [arXiv:0908.0212] [INSPIRE].

[14] J.L. Diaz-Cruz, *Holographic dark matter and Higgs*, *Phys. Rev. Lett.* **100** (2008) 221802 [arXiv:0711.0488] [INSPIRE].

[15] G. Giudice, C. Grojean, A. Pomarol and R. Rattazzi, *The strongly-interacting light Higgs*, *JHEP* **06** (2007) 045 [hep-ph/0703164] [INSPIRE].

[16] P. Gondolo and G. Gelmini, *Cosmic abundances of stable particles: improved analysis*, *Nucl. Phys.* **B 360** (1991) 145 [INSPIRE].

[17] WMAP collaboration, E. Komatsu et al., *Seven-year Wilkinson Microwave Anisotropy Probe (WMAP) observations: cosmological interpretation*, *Astrophys. J. Suppl.* **192** (2011) 18 [arXiv:1001.4538] [INSPIRE].

[18] C.E. Yaguna, *The singlet scalar as FIMP dark matter*, *JHEP* **08** (2011) 060 [arXiv:1105.1654] [INSPIRE].

[19] M. Frigerio, T. Hambye and E. Masso, *Sub-GeV dark matter as pseudo-Goldstone from the seesaw scale*, *Phys. Rev.* **X 1** (2011) 021026 [arXiv:1107.4564] [INSPIRE].

[20] LEP Higgs Working for Higgs boson searches, ALEPH, DELPHI, CERN-L3, OPAL collaboration, *Searches for invisible Higgs bosons: preliminary combined results using LEP data collected at energies up to* 209− *eV*, hep-ex/0107032 [INSPIRE].

[21] ATLAS collaboration, G. Aad et al., *Combined search for the standard model Higgs boson using up to 4.9 fb^{-1} of pp collision data at $\sqrt{s} = 7$ TeV with the ATLAS detector at the LHC*, *Phys. Lett.* **B 710** (2012) 49 [arXiv:1202.1408] [INSPIRE].

[22] CMS collaboration, S. Chatrchyan et al., *Combined results of searches for the standard model Higgs boson in pp collisions at $\sqrt{s} = 7$ TeV*, *Phys. Lett.* **B 710** (2012) 26 [arXiv:1202.1488] [INSPIRE].

[23] A. Falkowski, *Pseudo-goldstone Higgs production via gluon fusion*, *Phys. Rev.* **D 77** (2008) 055018 [arXiv:0711.0828] [INSPIRE].

[24] I. Low and A. Vichi, *On the production of a composite Higgs boson*, *Phys. Rev.* **D 84** (2011) 045019 [arXiv:1010.2753] [INSPIRE].

[25] A. Azatov and J. Galloway, *Light custodians and Higgs physics in composite models*, *Phys. Rev.* **D 85** (2012) 055013 [arXiv:1110.5646] [INSPIRE].

[26] XENON100 collaboration, E. Aprile et al., *Dark matter results from 100 live days of XENON100 data*, *Phys. Rev. Lett.* **107** (2011) 131302 [arXiv:1104.2549] [INSPIRE].

[27] DAMA, LIBRA collaboration, R. Bernabei et al., *New results from DAMA/LIBRA*, *Eur. Phys. J.* **C 67** (2010) 39 [arXiv:1002.1028] [INSPIRE].

[28] DAMA collaboration, R. Bernabei et al., *First results from DAMA/LIBRA and the combined results with DAMA/NaI*, *Eur. Phys. J.* **C 56** (2008) 333 [arXiv:0804.2741] [INSPIRE].

[29] C. Aalseth et al., *Search for an annual modulation in a p-type point contact germanium dark matter detector*, *Phys. Rev. Lett.* **107** (2011) 141301 [arXiv:1106.0650] [INSPIRE].

[30] CoGeNT collaboration, C. Aalseth et al., *Results from a search for light-mass dark matter with a p-type point contact germanium detector*, *Phys. Rev. Lett.* **106** (2011) 131301 [arXiv:1002.4703] [INSPIRE].

[31] G. Angloher et al., *Results from* 730 *kg days of the CRESST-II dark matter search*, *Eur. Phys. J.* **C 72** (2012) 1971 [arXiv:1109.0702] [INSPIRE].

[32] D. Hooper, *The empirical case for* 10 *GeV dark matter*, arXiv:1201.1303 [INSPIRE].

[33] C. Kelso, D. Hooper and M.R. Buckley, *Toward a consistent picture for CRESST, CoGeNT and DAMA*, *Phys. Rev.* **D 85** (2012) 043515 [arXiv:1110.5338] [INSPIRE].

[34] G. Jungman, M. Kamionkowski and K. Griest, *Supersymmetric dark matter*, *Phys. Rept.* **267** (1996) 195 [hep-ph/9506380] [INSPIRE].

[35] M. Cirelli et al., *PPPC 4 DM ID: a Poor Particle Physicist Cookbook for Dark Matter Indirect Detection*, *JCAP* **03** (2011) 051 [arXiv:1012.4515] [INSPIRE].

[36] P. Ciafaloni et al., *Weak corrections are relevant for dark matter indirect detection*, *JCAP* **03** (2011) 019 [arXiv:1009.0224] [INSPIRE].

[37] J. Lavalle, 10 *GeV dark matter candidates and cosmic-ray antiprotons*, *Phys. Rev.* **D 82** (2010) 081302 [arXiv:1007.5253] [INSPIRE].

[38] PAMELA collaboration, O. Adriani et al., *PAMELA results on the cosmic-ray antiproton flux from* 60 *MeV to* 180 *GeV in kinetic energy*, *Phys. Rev. Lett.* **105** (2010) 121101 [arXiv:1007.0821] [INSPIRE].

[39] S. Galli, F. Iocco, G. Bertone and A. Melchiorri, *CMB constraints on dark matter models with large annihilation cross-section*, *Phys. Rev.* **D 80** (2009) 023505 [arXiv:0905.0003] [INSPIRE].

[40] D. Feldman, Z. Liu and P. Nath, *PAMELA positron excess as a signal from the hidden sector*, *Phys. Rev.* **D 79** (2009) 063509 [arXiv:0810.5762] [INSPIRE].

[41] M. Ibe, H. Murayama and T. Yanagida, *Breit-Wigner enhancement of dark matter annihilation*, *Phys. Rev.* **D 79** (2009) 095009 [arXiv:0812.0072] [INSPIRE].

[42] W.-L. Guo and Y.-L. Wu, *Enhancement of dark matter annihilation via Breit-Wigner resonance*, *Phys. Rev.* **D 79** (2009) 055012 [arXiv:0901.1450] [INSPIRE].

[43] LAT collaboration, M. Ackermann et al., *Fermi LAT search for dark matter in gamma-ray lines and the inclusive photon spectrum*, arXiv:1205.2739 [INSPIRE].

[44] P.J. Fox, R. Harnik, J. Kopp and Y. Tsai, *Missing energy signatures of dark matter at the LHC*, *Phys. Rev.* **D 85** (2012) 056011 [arXiv:1109.4398] [INSPIRE].

[45] J. Goodman et al., *Constraints on dark matter from colliders*, *Phys. Rev.* **D 82** (2010) 116010 [arXiv:1008.1783] [INSPIRE].

[46] K. Cheung, P.-Y. Tseng, Y.-L.S. Tsai and T.-C. Yuan, *Global constraints on effective dark matter interactions: relic density, direct detection, indirect detection and collider*, *JCAP* **05** (2012) 001 [arXiv:1201.3402] [INSPIRE].

[47] J. Espinosa, C. Grojean and M. Muhlleitner, *Composite Higgs search at the LHC*, *JHEP* **05** (2010) 065 [arXiv:1003.3251] [INSPIRE].

[48] D. Carmi, A. Falkowski, E. Kuflik and T. Volansky, *Interpreting LHC Higgs results from natural new physics perspective*, arXiv:1202.3144 [INSPIRE].

[49] A. Azatov, R. Contino and J. Galloway, *Model-independent bounds on a light Higgs*, *JHEP* **04** (2012) 127 [arXiv:1202.3415] [INSPIRE].

[50] J. Espinosa, C. Grojean, M. Muhlleitner and M. Trott, *Fingerprinting Higgs suspects at the LHC*, *JHEP* **05** (2012) 097 [arXiv:1202.3697] [INSPIRE].

[51] J.R. Espinosa, T. Konstandin and F. Riva, *Strong electroweak phase transitions in the standard model with a singlet*, *Nucl. Phys.* **B 854** (2012) 592 [arXiv:1107.5441] [INSPIRE].

[52] J.R. Espinosa, B. Gripaios, T. Konstandin and F. Riva, *Electroweak baryogenesis in non-minimal composite Higgs models*, *JCAP* **01** (2012) 012 [arXiv:1110.2876] [INSPIRE].

[53] J. Kehayias and S. Profumo, *Semi-analytic calculation of the gravitational wave signal from the electroweak phase transition for general quartic scalar effective potentials*, *JCAP* **03** (2010) 003 [arXiv:0911.0687] [INSPIRE].

[54] D.B. Kaplan, *Flavor at SSC energies: a new mechanism for dynamically generated fermion masses*, *Nucl. Phys.* **B 365** (1991) 259 [INSPIRE].

[55] C.G. Callan Jr., S.R. Coleman, J. Wess and B. Zumino, *Structure of phenomenological lagrangians. 2*, *Phys. Rev.* **177** (1969) 2247 [INSPIRE].

[56] J. Mrazek et al., *The other natural two Higgs doublet model*, *Nucl. Phys.* **B 853** (2011) 1 [arXiv:1105.5403] [INSPIRE].

[57] K. Agashe, R. Contino, L. Da Rold and A. Pomarol, *A custodial symmetry for Zbb̄*, [*Phys. Lett.* **B 641** (2006) 62](https://doi.org/) [[hep-ph/0605341](https://arxiv.org/abs/hep-ph/0605341)] [[INSPIRE](https://inspirehep.net/)].

[58] R. Contino, L. Da Rold and A. Pomarol, *Light custodians in natural composite Higgs models*, [*Phys. Rev.* **D 75** (2007) 055014](https://doi.org/) [[hep-ph/0612048](https://arxiv.org/abs/hep-ph/0612048)] [[INSPIRE](https://inspirehep.net/)].

[59] H.-Y. Cheng and C.-W. Chiang, *Revisiting scalar and pseudoscalar couplings with nucleons*, [arXiv:1202.1292](https://arxiv.org/abs/1202.1292) [[INSPIRE](https://inspirehep.net/)].